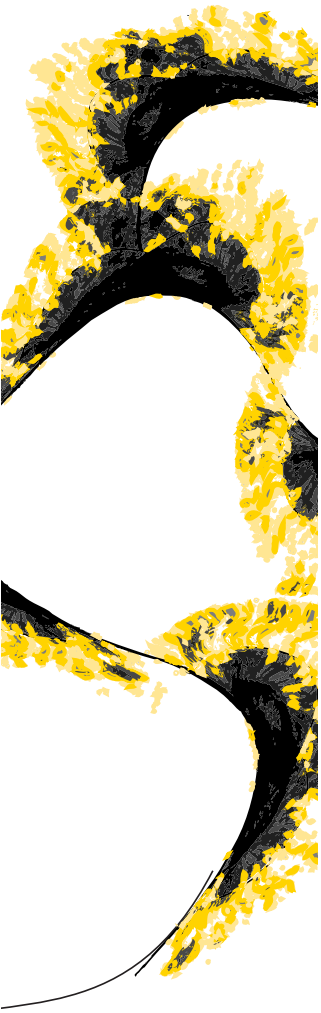

RAM ROBOTICS AND MECHATRONICS

IMPROVING THE DYNAMIC PERFORMANCE OF SEWER INSPECTION ROBOT

S.S. (Subham) Sutaria

MSC ASSIGNMENT

Committee:
dr. ir. J.F. Broenink
H. Noshahri, MSc
dr. ir. E. Dertien
dr. ir. L.L. olde Scholtenhuis

December, 2021

078RaM2021
Robotics and Mechatronics
EEMathCS
University of Twente
P.O. Box 217
7500 AE Enschede
The Netherlands

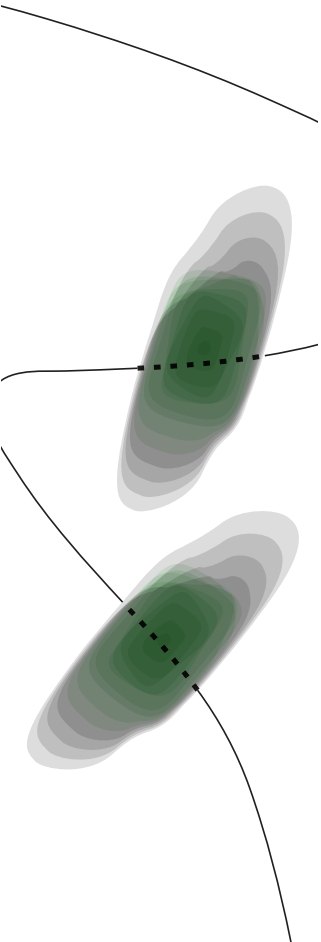

UNIVERSITY OF TWENTE. | TECHMED CENTRE UNIVERSITY OF TWENTE. | DIGITAL SOCIETY INSTITUTE

Summary

A significant challenge is appropriately maintaining the underground sewage systems with rapid urbanisation. Failure of sewage system causes service interruption, environmental damage, and pipeline collapse. It can be difficult to accurately locate and assess such a vast underground sewage system network. Thus, early inspection and assessment of the pipe condition are essential. One of the methods for detecting flaws in sewer pipes and voids around it is the impact-echo method. Man entry inspection is not possible since the sewer pipe diameter is about 300 mm to 600 mm. Also, visual inspection methods do not provide enough information about pipe structure defects and voids around the pipe.

Under the TISCALI (Technology Innovation for Sewer Condition Assessment – Long-Distance Information system) project, the Robotics and Mechatronics (RaM) group of the University of Twente has developed a robotic system to inspect the sewer pipes from inside using the impact-echo method. The impact-echo method includes three steps: stress-wave generation by an impact on the pipe wall, signal acquisition by a transducer, and data analysis of the recorded signal to detect deformities. The robot prototype mainly aims to perform the first step of the process. The type of the robot is a three-wheeled wall press that can make impacts all around the pipe. A manual inspection procedure is programmed in the Arduino IDE software. The robot prototype has performance issues in structural robustness, automated control and robot portability. Also, the repeatability and reliability of the impact-echo test were not enough.

This thesis focuses on improving the overall performance of the inspection robot. The robot includes a centering mechanism to center the robot inside the pipe, a lifting mechanism to place the impact-echo setup close to the pipe wall, and a rotating mechanism to rotate the impact-echo setup inside the pipe. Mechanical design of the centering mechanism and lifting mechanism is improved to increase the robot's stability and reliability of the impact-echo test. Feedback control for lifting mechanism using a distance sensor and rotating mechanism using angle sensor is implemented to improve the repeatability and precision of the impact-echo tests. A semi-automated control routine is developed to automate the inspection procedure and remove human errors. Hardware component optimisation is carried out to make the robot more portable.

The experiments are carried out in a 400 mm PVC pipe. The results show that the centering mechanism still does not center the robot inside the pipe. It remains short by 15 mm. The results of the lifting mechanism show that the distance of 40 mm between the impact-echo setup to the pipe wall is achieved, and its repeatability is sufficient to perform impact-echo test multiple times. The impact-echo setup can be oriented at any desired angle inside the pipe. The rotating mechanism shows an error of $\pm 1^{\circ}$ for the initial rotation, but then the feedback control corrects the final angle. The average inspection procedure time with the semi-automatic control routine for inspecting a particular section of the pipe is about 2 minutes. A transducer can be placed near the impact point to capture the echo generated by the stress wave. Overall, the performance of the sewer inspection robot has been improved in terms of uniqueness and consistency of the impact-echo test, structural rigidity, and automated control.

Contents

List of Figures

1 Introduction

1.1 Context

A considerable challenge in the urbanizing world of the 21st century is the proper maintenance and rehabilitation of underground utilities such as gas/water pipelines, electricity, telecommunication/fibre optic cables and sewage systems. The lack of accurate and sufficient information about this vast multi-layer underground network has made localizing and assessing the condition of each utility difficult (Dertein, 2015). Sewage system maintenance has the highest service interruption, environmental damage, cost, and pipeline collapse among the underground urban assets.

The Technology Innovation for Sewer Condition Assessment – Long-Distance Information-system (TISCALI) project aims at utilising, integrating, and further developing relatively low-cost, off-shelf techniques to arrive at an accurate detection and quantification of defects in sewers and to determine the constructive strength and stability of sewers. This project collaborates with three faculties: the University of Twente, namely, EWI, CTW, and ITC and industrial partners. In collaboration with Department of the Construction Management and Engineering, RaM is responsible for the Assessing Sewer Condition (ASC) sub-project. The goal is (a) To quantify the sewer condition locally using an in-pipe robotic inspection, and (b) To build a smart subsurface information system, or toolkit, that supports objective sewer condition assessment.

A part of this project is to develop an in-pipe inspection robot that can help detect cracks in the pipe structure, voids around the pipe, measure the thickness of the sewer pipe, and generate 'early warnings' for failure. Structural deformities such as cracks in the sewer pipe may lead to water leakage out of the sewer pipe or groundwater seeping inside the sewer pipe through the soil around it. In either case, the soil around the pipe gets washed away and thus create small voids. These voids get bigger over time and loosen the soil around the sewer pipe. Due to moving traffic on the road above the sewer system, the chances of the sewer pipe collapsing are high because of the weak foundation (Davies et al., 2001).

Currently, many non-destructive testing methods are available to inspect concrete structures. These methods detect internal defects such as voids, cracks, delaminations, etc (Bin Ibrahim et al., 2002). Out of these methods, the impact-echo method is widely used in civil engineering for the assessment of concrete structures (Noshahri et al., 2021). The motivation for this project arises from the need to develop a robotic system to inspect fissures and defects in the concrete sewer pipes using the impact-echo method.

1.2 Problem Description

Within the context mentioned above, a crawler robot with the impact-echo test setup was developed in the RaM lab by Dr Edwin Dertien, as shown in Figure 1.1. The impact-echo method comprises of generating stress waves using a short duration mechanical impact and a transducer to monitor the surface displacement due to the arrival of direct and reflected stress waves (Carino, 2015). The impact echo method has three main steps: stress wave generation, signal acquisition, and data analysis. The crawler robot aimed to make an impact (tap) inside the pipe, and a separate setup was used to capture the echo generated by the impact and then analyse it. Figure 1.1 shows the crawler robot in a concrete sewer pipe. It could only make an impact in a 300 mm pipe which is smaller than what is shown in the figure. To inspect a pipe section thoroughly, an impact needs to be made at multiple points along the whole circumference of the pipe. The limitation of this crawler robot is that it can make only one impact on the circumference of the pipe, which is not enough to inspect the pipe entirely.

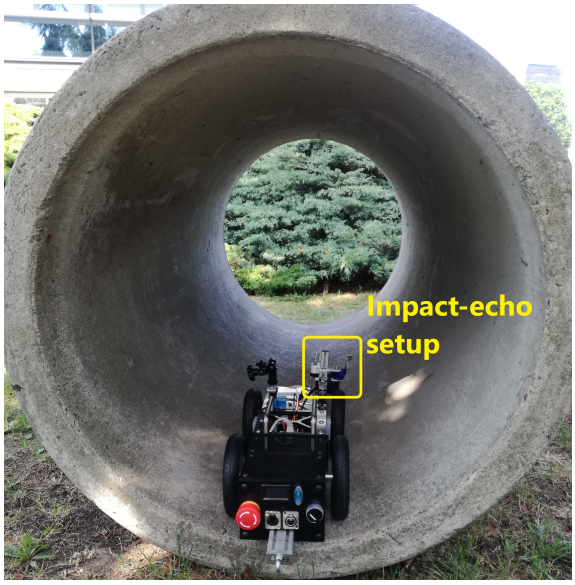

Figure 1.1: Crawler robot with impact-echo setup

Therefore, the impact-echo test setup was shifted to a new in-pipe inspection robot prototype that was developed by Zwiep (2021) in the RaM Lab. The prototype is a wheel wall-press type in-pipe inspection robot as shown in Figure 1.2. The purpose purpose of this prototype in the whole impact-echo method is to generate the stress wave. The features of this prototype are that it can operate in variable pipe diameters ranging from 300 mm to 500 mm, it can make an impact at 4 points on the inner circumference of the sewer pipe.

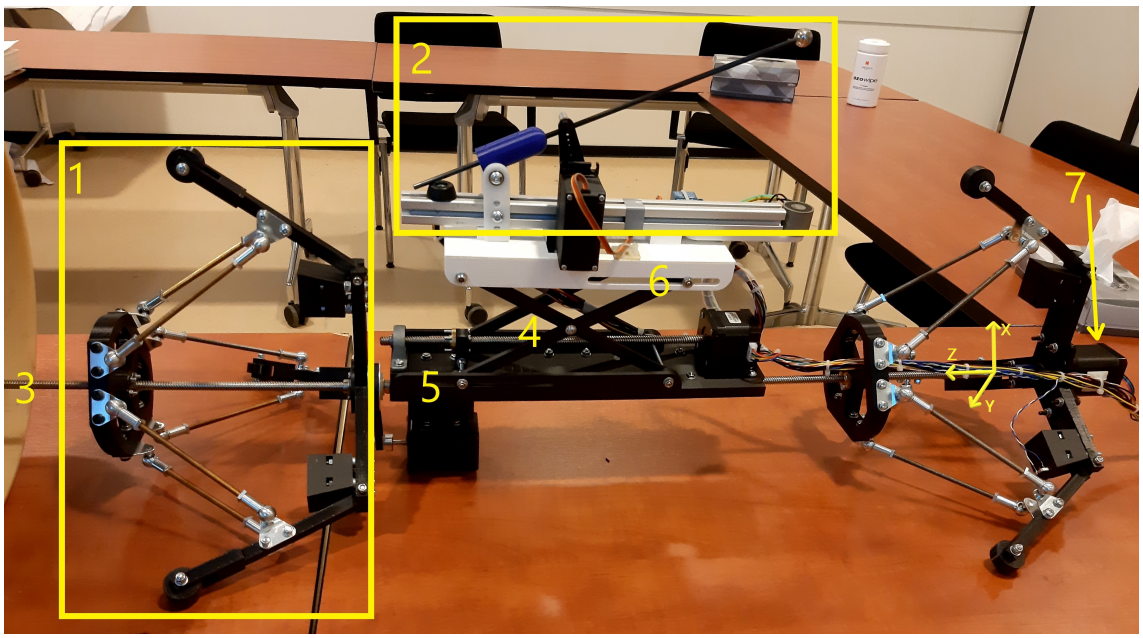

Figure 1.2: Overview of the current setup
1. centering mechanism 2. Impact-echo setup 3. Center lead screw 4. Scissor lifting mechanism 5. Rotating mechanism 6. Impact-echo setup platform 7. Centering stepper motor

An overview of the prototype is discussed here. Assume the X-, Y-, Z-axis of the prototype as shown in Figure 1.2 to understand the prototype. The whole robot structure is mounted on a lead screw shaft (part 3 in Figure 1.2), which is considered along the Z-axis. The centering mechanism shown as part 1 in Figure 1.2 expands and retracts to adapt to different pipe diam-

eters. The impact-echo setup (part 2 in Figure 1.2) is mounted on a platform (part 6 in Figure 1.2) that is operated by a scissor lift mechanism (part 4 in Figure 1.2). The scissor lifting mechanism puts the impact-echo setup at a desired distance from the sewer pipe wall. A rotation mechanism rotates the impact-echo setup to make an impact at different angles on the circumference of the pipe. The orientation of the impact-echo setup shown in the Figure 1.2 as considered as 0°. Looking from the centering stepper motor (part 7 in Figure 1.2) side, clockwise rotation is considered as a negative and counter-clockwise rotation as positive. Detailed analysis of the prototype is given in Chapter 2.

Despite this prototype being able to make impacts at multiple angles inside the pipe, the reliability and uniqueness of the impact test are not achieved. The overview of the requirements and shortcomings of this prototype is discussed below:

- The Overall structure of the robot is weak because the whole structure relies on a lead screw and there are not enough supports at the middle part where the lifting mechanism lies.
- To make an impact at every angle inside the pipe, enough space needs to be there for the movement of the rotation mechanism. And for that, the centre lead screw needs to be at the center of the pipe, ensuring the impact-echo setup remains equidistant from the pipe wall. The problem with the prototype is that it can not center itself inside the pipe.
- The impactor needs to hit the wall with a certain amount of energy, and for that, the distance of a point from where the impactor is released to the pipe wall needs to be maintained for every impact-echo test. But this prototype is not able to maintain that distance every time.
- While testing a section of the pipe, it is essential to know the angle of impact, and it needs to be maintained. In the current prototype, the rotation mechanism controls the angle of impact. But as the control method is open-loop control, it is not possible to track the angle of impact and maintain it.
- Feedback control is required for the repeatability and reliability of the impact-echo test. The current control method is open-loop control i.e., manually controlled by an operator. It is prone to human errors. So, it is not a reliable control method for inspection.
- Electronics component placement and wiring play a vital role in the portability of the prototype. As the inspection robot needs to be transported to a place of inspection, the portability of the robot is required. The current prototype lacks this feature.

1.3 Goals

The main aim of this thesis is to improve the performance of the current robot prototype. Performance improvement includes identifying the design flaws of the current robot prototype and improving it, implementing closed-loop control to different robot mechanisms and optimizing the hardware components to make the robot prototype portable. As the primary purpose of this prototype is to generate stress waves, the signal acquisition and data analysis part of the inspection process is out of scope for this thesis. To address the problems mentioned above, goals are defined as:

- Make the centering mechanism robust.
- Implement feedback control for different mechanisms of the robot.
- Develop an automated inspection procedure and a program code for the same.

- Identify the design problems/ flaws in the robot and correct them if necessary.
- Minimise the electronics and optimize the wiring to make the robot portable.

These goals are classified to have design objectives for this thesis in the following chapter.

1.4 Assumptions

A few assumptions are made for this thesis to make it more feasible in the allocated time. These assumptions are listed below:

- The experimental setup of sewer pipe is clean from inside.
- The sewer pipe is straight and is kept on a flat ground.
- The inner diameter of the sewer pipe is constant along the length of the pipe.
- The pipe does not have any lateral connections and the inner surface of the sewer pipe is uniform.

1.5 Thesis outline

In chapter 2, a comparison of different pipe inspection robots, a detailed analysis of the previous prototype, and design objectives for this thesis are given. Chapter 3 elaborates on the mechanical design choices, component selection and optimal placement, and the control algorithm for the test procedure. Chapter 4 includes the experimental test results and provides the discussion. Chapter 5 consists of the conclusions and further recommendations.

2 Analysis

This chapter compares the design of in-pipe inspection robots related to the type of pipe inspection robot used for the TISCALI project. The comparison is carried out mainly to explore the centering mechanism design and analyse the possibility of implementing it in the current prototype. Next to that, the impact-echo method is explained from the point of view of stress wave generation. Lastly, a detailed explanation of the working procedure of the current prototype is discussed, and challenges with the current prototype are explained.

2.1 Comparison of pipe inspection robots

This section compares the centering mechanism of wheeled wall-press type pipe inspection robots to improve their structural robustness. It is linked to the goal 1.3. The Appendix A gives an overview of different types of in-pipe inspection robots according to their applications. The centering mechanism mechanism of these robots help them to fit inside the pipe and allow them to move inside the pipe. Apart from analysing the pipe adaption mechanism of different inspection robots, this comparison also analyses the feasibility to implement the impact-echo test setup on that robot design and compatibility for pipe diameter. Feasibility to implement the impact-echo test setup consists of checking if there is enough space to fit the impact-echo setup with a mechanism to vary its height.

1. Figure 2.1 (Min et al., 2014) shows a wheeled wall-press type robot. It is suitable for 300 mm to 500 mm pipe diameter with multiple elbows in the pipe. It has three rubber wheel pair configurations. A motor powers each wheel pair to move the robot in the pipe. For expansion and retraction of wheels, a 4-bar linkage is provided, which is connected to a shaft holder. The shaft holder slides on a threaded shaft rotated by a high torque DC motor and gear mechanism. This module is called an active module. Impact-echo test setup can be mounted on a platform in-between two active modules. However, rotating the test platform inside the pipe would require a different mechanism. The advantage of this design is its structural robustness. Experiment results showed that the design works well in 300 mm pipe. This centering mechanism design can be scaled up to implement in the current prototype.

Figure 2.1: Design 1 (Min et al. (2014))

2. Figure 2.2 (Feng et al., 2016) shows a wheeled wall-pressing type in-pipe cleaning robot suitable for large pipe diameters (ϕ 1200 - ϕ 1500 mm). This design also has a pair of 3 wheels at 120° apart from each other. A motor powers each wheel pair. This robot also fits inside different pipe diameters with expansion and retraction of the centering mechanism. All three legs of the centering mechanism are operated by a separate lead screw sliding nut pair. Springs support the swing rod on which wheels are mounted. Thus, each leg can be controlled separately. These individual mechanisms increase the robot's weight and require high torque motors for the centering mechanism. The simulation experiments performed in a 1400 mm water pipeline showed that the normal force exerted by the driving wheels on the pipeline wall is enough to guarantee complete contact. This design is not feasible to mount the impact-echo test setup because a separate mechanism needs to be designed to rotate it, making it complicated to implement.

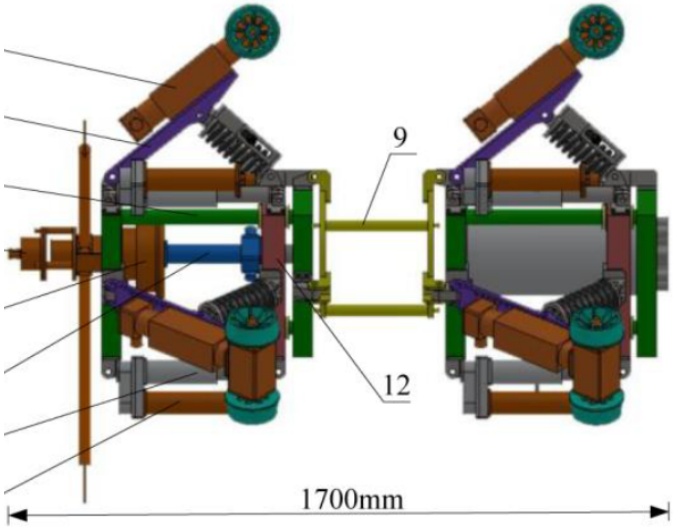

Figure 2.2: Design 2 (Feng et al. (2016))

3. Figure 2.3 (Kakogawa and Ma, 2010) shows a screw-motion type inspection robot suitable for smaller diameter pipelines. There are two modules: stator and rotator. A DC motor rotates the rotator, and the stator drags along the pipe. The rotator wheels mounted at 120° from each other are placed at an inclined angle so that the rotator follows a helix path along the pipe length. Wheels are attached by a spring with the arm to move in curved pipes quickly. It has a relatively straightforward drive mechanism as only one motor is required to drive the robot. It is difficult to put the impact-echo test setup on this type of robot because of the power delivering mechanism of the robot. As the length of the robot increases to accommodate the impact-echo test setup, it would be difficult to provide power with a single motor. Secondly, this design is not suitable for the significant variation in pipe diameter.

4. Figure 2.4 (Zhang and Yan, 2007) shows a wheeled wall-press type pipe inspecting robot suitable for gas pipelines with different diameters. It has three sets of parallelogram wheeled leg mechanisms which are circumferentially spaced at 120° apart symmetrically. This structure actively adapts to pipe diameters ranging from ϕ 400 mm to ϕ 600 mm and has an automatic tractive force adjustment. Tractive force is determined by the adhesion force, which depends on the normal pressure and adhesion coefficient between driving wheels and pipe wall. A chain connects the front and rear driving wheels to expand and retract simultaneously. The experiments performed in different pipe diameters showed that the tractive force's measured output under the control strategy used was near what

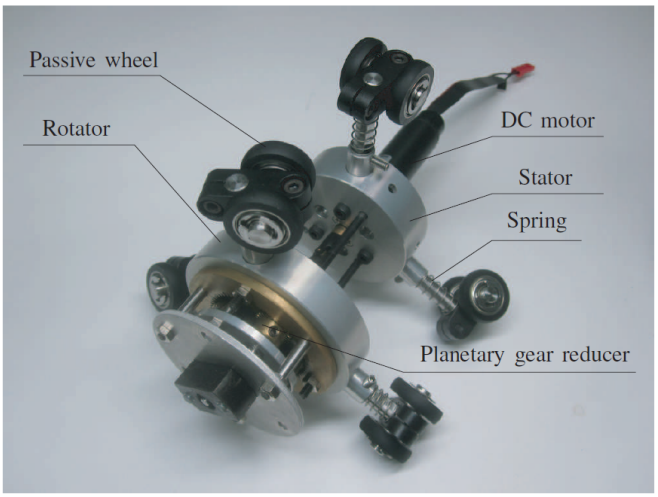

Figure 2.3: Design 3 (Kakogawa and Ma (2010))

was expected. Tractive force adjustment is a good feature that can be used for the current robot prototype. One problem with implementing this design is that the rotation feature of the current setup will be removed. An alternate way of having rotation can be by rotating the whole robot inside the pipe.

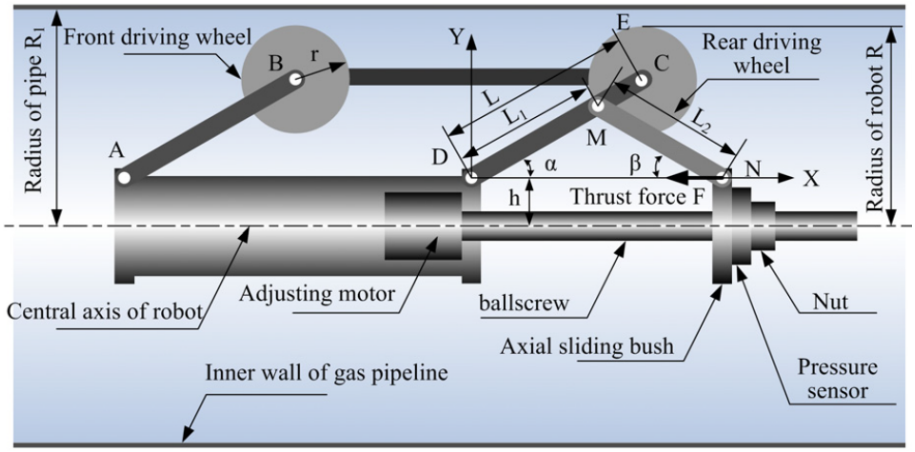

Figure 2.4: Design 4 (Zhang and Yan (2007))

5. Figure 2.5 (Wahed and Arshad, 2017) again shows a wheeled wall-press type robot suitable for a smaller pipe diameter range between ϕ 150 mm to ϕ 230 mm. This robot has two parts: a camera module in the front and a driving module with two identical sections of expanding and retracting legs to adjust different pipe diameters. Unlike other designs discussed so far, the arm on which wheels are mounted have only single support to the main body. The same lead screw and nut mechanism are used for expanding and retracting legs in the above designs. Here, also the driving wheels are powered by a motor. The robot is fabricated from 3D printed parts. The experiments concluded that this design works in variable pipe diameter but does not work in actual pipe conditions because the material used for manufacturing did not provide enough strength. Due to the robot's weight, the legs can bend without support to the main body. So, this design is also not suitable to implement in the current prototype.

One common thing about all these designs, apart from Design 5, is that the parts used for developing the pipe inspection robot are made from metal which provides structural strength.

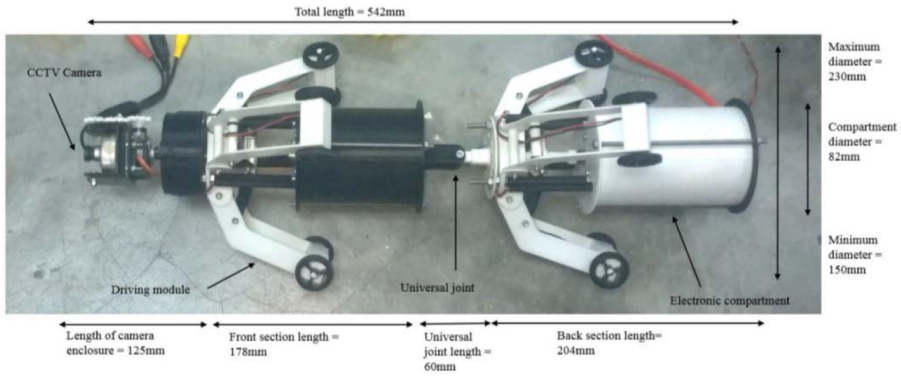

Figure 2.5: Design 5 (Wahed and Arshad (2017))

But for this thesis, 3D printed parts are used because the pipe inspection robot is still a prototype and not the final design. The other common thing is that all these designs have a wheel pair for each leg, which increases the contact points between the robot and the pipe wall and improves the robot's stability. Also, wheels in all the designs are driven by motors, which is not present in the current prototype. The feasibility of implementing the impact-echo setup is not the same for every design discussed above. These robots have a different range of compatibility of pipe diameters. Based on this comparison, the design changes required to make the centering mechanism robust are discussed in Chapter 3. But before that, a detailed analysis of the current prototype is needed, carried out in the following section.

2.2 Analysis of the current prototype

The starting point of this thesis with the in-pipe inspection robot prototype made by Zwiep (2021). A brief overview is already given in Chapter 1. This section includes an in-depth analysis of the current prototype with its manual control algorithm used to control it and issues with the prototype.

Figure 2.6 shows the current setup of pipe inspection robot with description of every part. There are mainly four mechanisms in this prototype: impactor (tapping) mechanism, centering mechanism, lifting mechanism, and rotating mechanism. Except for the impactor mechanism, operated by a servo motor, all other mechanisms are operated by stepper motors. Their stepper motor driver, TB6600, drive all the stepper motors. All stepper motor and electromagnet operates on 12 V DC, and the servo motor operates on 6 V DC. Two separate power sources are used for this. All the stepper motor drivers and Arduino are placed in an electronic box.

The control algorithm for the working procedure is programmed in Arduino MEGA ADK and is operated by a Logitech gamepad controller. The working procedure of the pipe inspection robot is shown in the form of a flowchart in Figure 2.7. In the flowchart, the stepper motor for centering, lifting and rotating mechanisms are referred to as 1, 2, 3, respectively. The control method is an open-loop control. For every task of the working procedure, a button on the Logitech gamepad controller is assigned. The description of which button of Logitech controller does what is given in Appendix D. The manual working procedure is explained below:

- Initially, homing of all mechanisms is carried by pressing the Start button once. Description of tasks involved in homing is shown in Figure 2.7.
- Then, the centering of the robot is carried out by rotating the centering stepper motor in the clockwise direction. There are no pre-defined step counts for any stepper motors; it rotates in a particular direction until the corresponding button is pressed. All stepper motors are controlled manually by looking at the robot in the pipe.

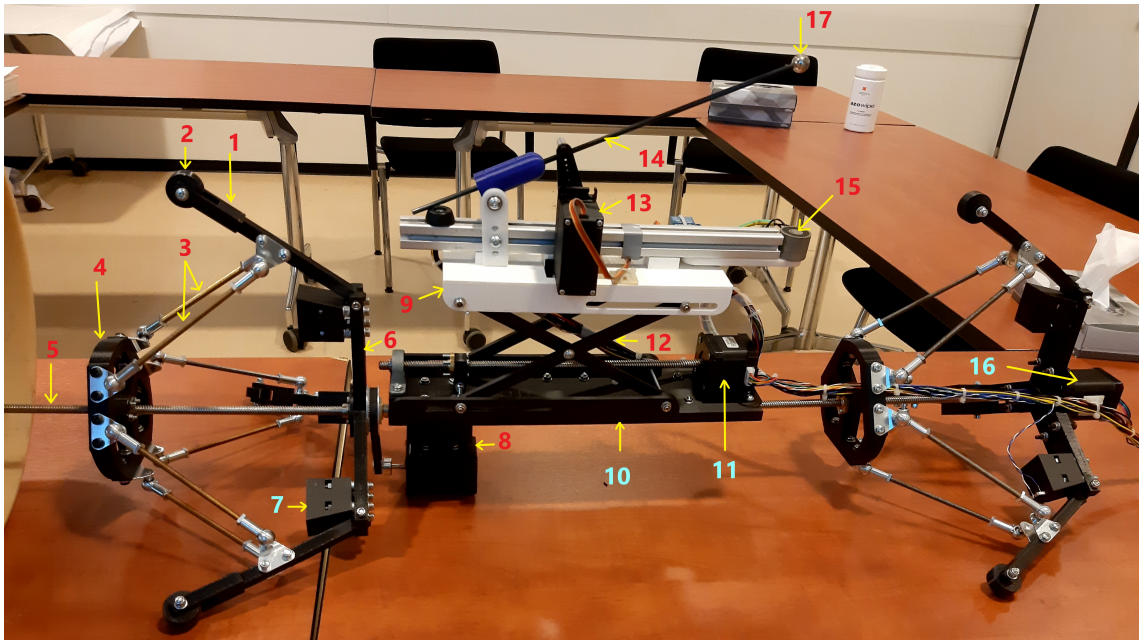

Figure 2.6: Current prototype of in-pipe inspection robot (Zwiep, 2021)
1. Dynamic leg 2. Roller 3. Supporting links 4. Thread shaft nut mount 5. Thread shaft 6. Static leg 7. stopper block 8. Rotation stepper motor 9. Top plate 10. Base plate 11. Lifting stepper motor 12. Scissor links 13. Servo motor 14. Impactor arm 15. Electromagnet 16. Centering stepper motor 17. Impact ball

- After centering, lifting the impact-echo setup is done using the lifting mechanism. It raises the top plate to a height where the impact-echo test can be carried out. The height of the lifting mechanism is adjusted manually.
- Then, the impact test is performed. A brief overview of the impact-echo method and important parameters of the test setup, used for this thesis, is given in Appendix A. The procedure for making an impact is first by putting the impactor arm towards the magnet and simultaneously turning on the magnet, then placing the servo to start position, then turning off the magnet. As soon as the magnet is turned off, an impact is made. Lastly, the impactor arm is put to its homing position, horizontal to the ground. All the servo motions are calculated based on approximation of the arm movement. The echo generated by the impact is captured by a transducer (mic) placed close to the impact. And later, it is analyzed to identify the deformities in the pipe or voids around the pipe.
- After making an impact at a point in the pipe, the de-lifting of the lifting mechanism is carried out until the top plate completely sits down on the base plate.
- Then, to perform the impact on another angle on that circumference of the pipe, the mechanism is rotated using a rotating mechanism. The direction of the rotation mechanism is the same as the direction of the rotating stepper motor. It is rotated based on a visual approximation of the angle.
- After the rotation, the same procedure from lifting to de-lifting is performed again to make an impact on the pipe wall.
- After making four impacts at every 90° on the inner circumference of the pipe, the inspection of that section of the pipe is completed. Lastly, de-centering of the robot is carried out.

This working procedure is followed to inspect a particular section of the pipe. As the robot can not move forward or backward inside the pipe by itself, a separate robot pushes it further to

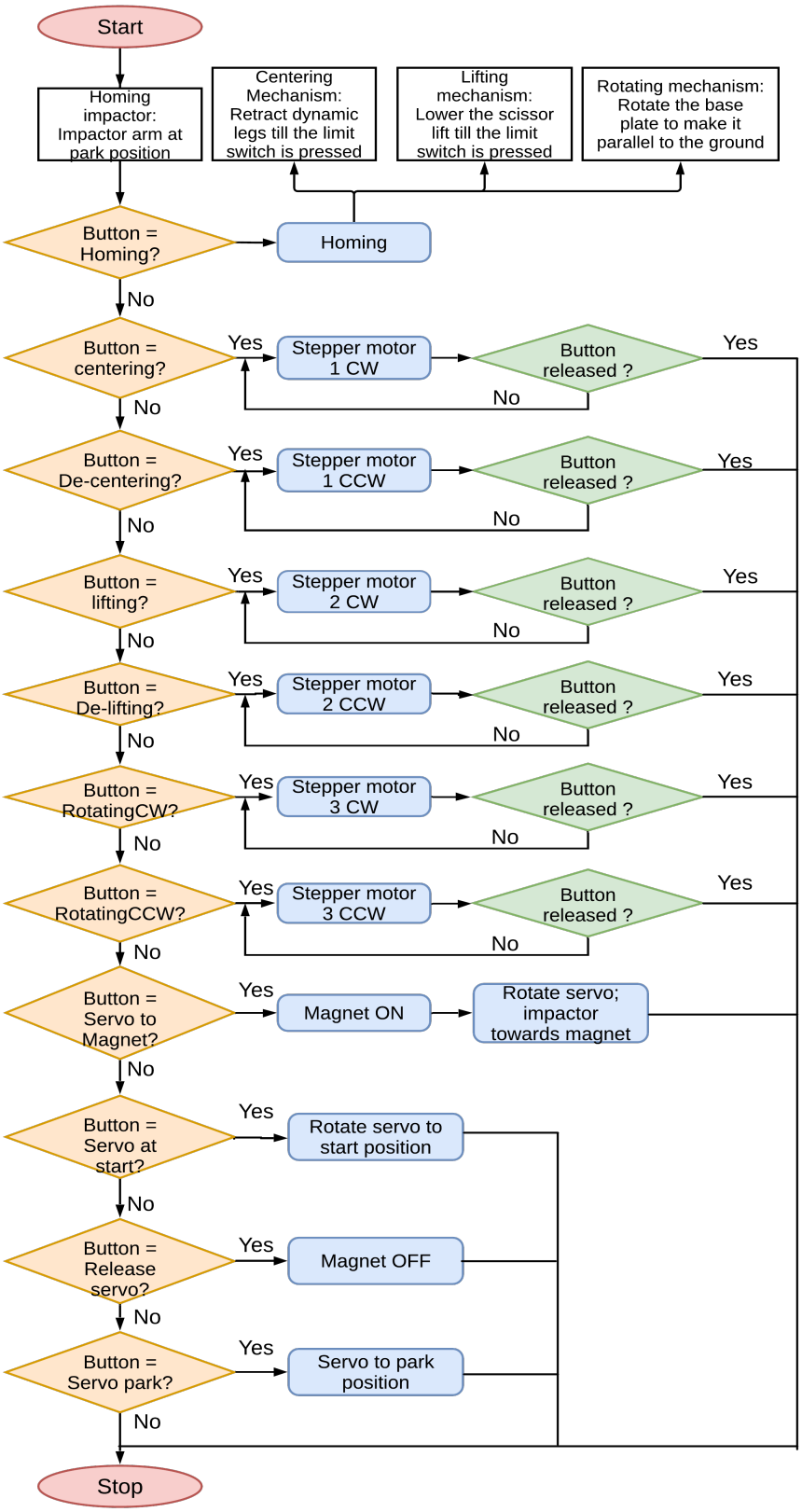

Figure 2.7: Manual routine flowchart of the current prototype

inspect the next section and pulls out of the pipe when the inspection is complete. The robot used for this purpose is the crawler robot mentioned in Chapter 1.

This prototype requires improvement in certain aspects like mechanical structure, automated control and optimization of electronic components. All these problems are discussed in detail.

First of all, the robot cannot effectively center itself inside the pipe. The purpose of the centering mechanism is to lift the robot and align the central lead screw with the center of the pipe. The problem starts with the material used for fabricating the dynamic legs. It is not strong enough to provide the push force required to expand the legs to fit in the pipe. It tends to bend from where it connects to the supporting links when the dynamic legs are expanded in the pipe. In addition to that, the roller wheels create sliding friction when dynamic legs are expanded. The sliding friction constrains the leg movement and does not allow the legs to expand smoothly. Also, there is mechanical play in the joint connecting the dynamic leg with the static leg. These all add up and does not allow the robot to center itself in any pipe size.

The second problem is with the lifting mechanism. The connection of the scissor links with the top plate, and the base plate is loose, which again creates a lot of mechanical play in the structure. This play generates a problem when the base plate is rotated on either side (see figure 2.8). Part 2 of Figure 2.8 is the top plate (white), and it shows that it is not aligned with the base plate. This tilting of the top plate makes it difficult to determine the exact angle at which the impact will be made.

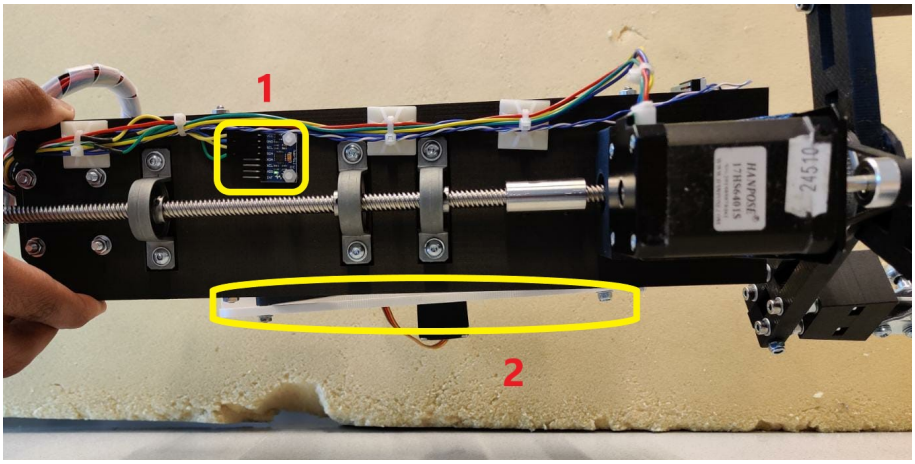

Figure 2.8: Bottom view of base plate when rotated by 90°
1. MPU-6050 angle sensor 2. Tilting of the top plate due to play in the joints

The third problem comes with the length of the robot. The whole structure relies on a single lead shaft of 8 mm, and there is no support for the base plate to the ground. So, the lead shaft tends to sag because of the weight. Sagging also makes the center part wobble a bit when its impact. It disturbs the stability of the whole structure of the pipe. Because of the sagging, it is difficult to maintain a fixed distance from the top plate to the pipe wall. Sagging creates more problems when the impact-echo setup is at 90° or 180°.

The fourth problem is the lack of control of the lifting platform. As the scissor lift mechanism is operated manually, placing the impact test setup at a particular distance from the pipe wall is not possible every time. For consistent results, it is required to place the impact test setup at the same position as the pipe wall.

The fifth problem is with the electronics and the wiring. All the electronics are placed in a box kept away from the robot. It gets complicated to manage the wiring when setting up the robot in the pipe. The length of the wire is concise, which does not allow placing the robot further inside the pipe.

All these problems lead to the overall poor performance of the inspection robot. To resolve the issues mentioned above, re-designing some parts of the prototype is required, implementing an automated control is required using new sensors, and optimizing the electronics is required.

So the following chapter will focus on all these problems and resolve them by redesigning parts of the robot, adding and replacing some components to automate the test procedure and optimizing the electronics and wiring.

2.3 Requirements

Based on the problems mentioned above and aligned with the goals discussed in section 1.3, the requirements are prioritized according to the MoSCoW prioritization method. MoSCoW represents four categories: must-have, should-have, could-have and won't-have or will not have. This method is chosen because it helps in systematically prioritizing the requirements. The 'must-have' objectives are derived from the significant problems mentioned in the above section. The 'should-have' objectives come from minor issues, and it is still necessary to resolve them. The 'could-have' objectives are decided based on less important tasks, which, even if not achieved, will not much affect the overall performance of the pipe inspection robot. The 'will not have' objectives are out of the scope for this thesis and are future recommendations for this project. The design objectives are shown below:

- Must have
  (a) Make the robot centering mechanism robust.
  (b) Place the impact-echo setup at specific distance from the sewer pipe wall.
  (c) Implement precise movement control for the rotation of impact-echo setup.
  (d) Develop an automated impact-echo test procedure.
- Should have
  (a) Effective centering of the inspection robot with the center of sewer pipe.
  (b) Minimize the tilting of the lifting platform when rotated.
  (c) Minimize the electronics and wiring to transport the robot with ease.
  (d) Improve the wheel design to reduce the friction between wheels and pipe wall.
- Could have
  (a) Minimize sagging of middle part of the robot (see figure 1.2).
  (b) Mobilize the robot by adding motor to the wheels.
- Will not have
  (a) Add a camera on the robot to have visuals of the sewer pipe.
  (b) Check the possibility to re-design the impactor mechanism so that overall length of the robot can be reduced and sagging of the middle part can be eliminated.

According to these requirements, the proposed new design of the prototype, implementation of new sensors for automated control and an improved working procedure of the inspection robot is described in Chapter 3.

3 Design & Implementation

This chapter covers the re-design of centering mechanism and the lifting mechanism to overcome challenges mentioned in the previous chapter, implementing hardware and software to automate the working procedure of the prototype. Design changes are made on the prototype created by Zwiep (2021) to improve its performance. From this chapter, the current prototype is referred to as 'previous prototype', and the newly designed prototype is referred to as 'new prototype'.

3.1 Design of centering mechanism

This section describes the new proposed design of the centering mechanism. The essential parts of the centering mechanism which need to be redesigned are dynamic leg, wheels, and supporting links. First, the design is made in Solid Works software, and then parts are 3D printed. These fabricated parts are installed on the previous prototype replacing the corresponding old parts. The criteria that need to be checked are: no bending of the dynamic leg when expanded or retracted inside the pipe, minimum friction between wheels and pipe wall, the dynamic leg can be expanded to adapt in pipe size from 300 mm to 500 mm, and the centering mechanism should be able to align the central axis of the robot with the center of the pipe.

The figure shows the Solid Works model of the new design of centering mechanism. The wheels are re-designed to have minimum friction with the pipe wall. The design of supporting links are changed to have a simplified connection between lead screw nut mount and dynamic leg. The important design change is for the dynamic leg. The new design has improved joint with the static leg.

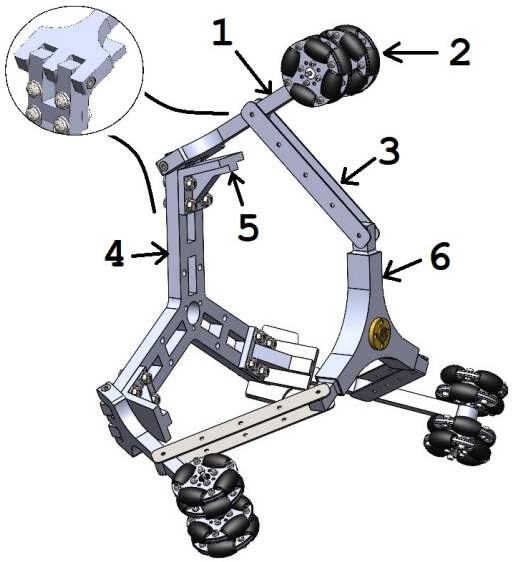

Figure 3.1: New design of the centering mechanism
1. Dynamic leg 2. Omni wheel 3. Supporting link 4. Static leg 5. Supporting block 6. lead screw nut mount

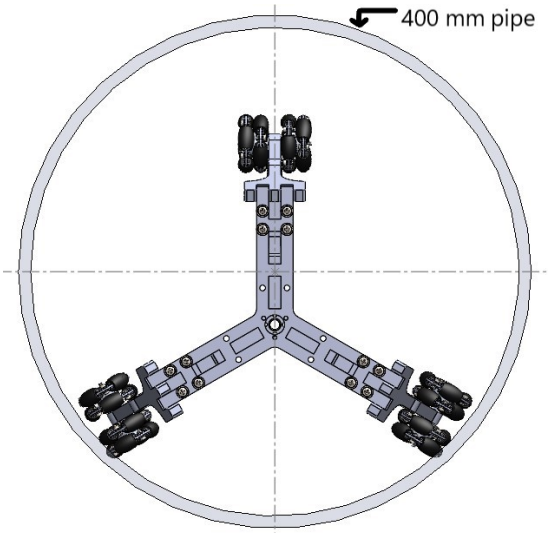

Figure 3.2: Initial configuration of the centering mechanism inside a pipe

The reason for a new design of dynamic leg is to improve the joint between the dynamic leg and static leg (part 4 in Figure). The joint between the dynamic leg and static leg needs to have only 1 degree of freedom (DOF), i.e., about the rotating axis. But the dynamic leg design of

the previous prototype (part 1 in Figure 2.6) is not able to constrain the joint motion to 1 DOF because of mechanical play in the joint. Thus, a hinge structure of the dynamic leg (zoomed section of part 2 in the Figure 3.1) is designed, which provides more contact area with the static leg and thus restricts the joint motion to 1 DOF. To provide more structural strength to the dynamic leg, the material used for the dynamic leg is Nylon with carbon fibre which offers more strength than the ABS plastic material used in the earlier design. The length of the dynamic leg is kept the same as the previous design. Bearings are used for the joints to reduce friction.

The wheel design is changed from a small roller (part 2 in Figure 2.6) to a Omni wheel (part 2 in Figure 3.1). Omni wheels have small rollers around the circumference perpendicular to the turning direction, so they can also slide laterally with ease. The free lateral movement of the Omni wheel is the reason for its selection. The initial position in which the robot is placed inside the pipe is shown in Figure 3.2, with two dynamic legs in contact with the pipe wall. As the centering mechanism starts to expand, the small roller of the Omni wheel allows free lateral movement. The diameter of the Omni wheel is 48 mm. It is the optimum diameter of the wheel so that even with the centering mechanism completely retracted; the wheel is in contact with the pipe wall. The sliding friction of the roller in the previous design is more than the rolling friction of the Omni wheel. A pair of two wheels are added to the new design to provide more contact points with the pipe wall, increasing grip of the robot on the pipe wall. Initially, only one of the Omni wheels is in contact with the pipe wall, as can be seen from the Figure 3.2, but as the centering mechanism starts to expand, both the wheels come in contact with the pipe wall. The Omni wheels are made in the lab. Rim plates of the wheels are laser cut, and the rollers are 3D printed. The rollers are made up of 2 different materials: the inner part is PLA, and the outer part is rubber. Rubber material provides a good grip on the pipe surface.

The supporting link (part 3 in Figure 3.1) design is changed from triangle-shaped support (part 3 in 2.6) to a simpler design in which a pair of thin metal plates placed parallel to each other are connected between the dynamic leg and the lead screw nut mount (part 6 in Figure 3.1). This design was chosen to directly support dynamic leg and lead screw nut mounts. It was inspired by design in Min et al. (2014). The length of the supporting link is 130 mm, which is equal to the distance from the dynamic leg to the lead screw nut mount in the previous prototype.

3.1.1 Calculation for required torque

The required torque for the centering mechanism calculated here is taken reference from Zhang and Yan (2007). The schematics of the centering mechanism is shown in the Figure 3.3. The figure shows one of the three similar link arrangements in the centering mechanism, all spaced at 120° from each other.

In the figure 3.3,

R = radius of the robot;
R_1 = radius of the pipe;
H_1 = height from the central axis of the inspection robot to supporting point D;
H_2 = height from the central axis of the inspection robot to supporting point N;
r = radius of the wheel;
L = length of the link CD (dynamic leg);
L_1 = distance between point D and point M;
L_2 = length of the link MN (supporting link);
α = included angles between link CD and the axis X;
β = included angles between link MN and axis X;
F = thrust force of mechanism motion which is caused by the lead screw and nut pair

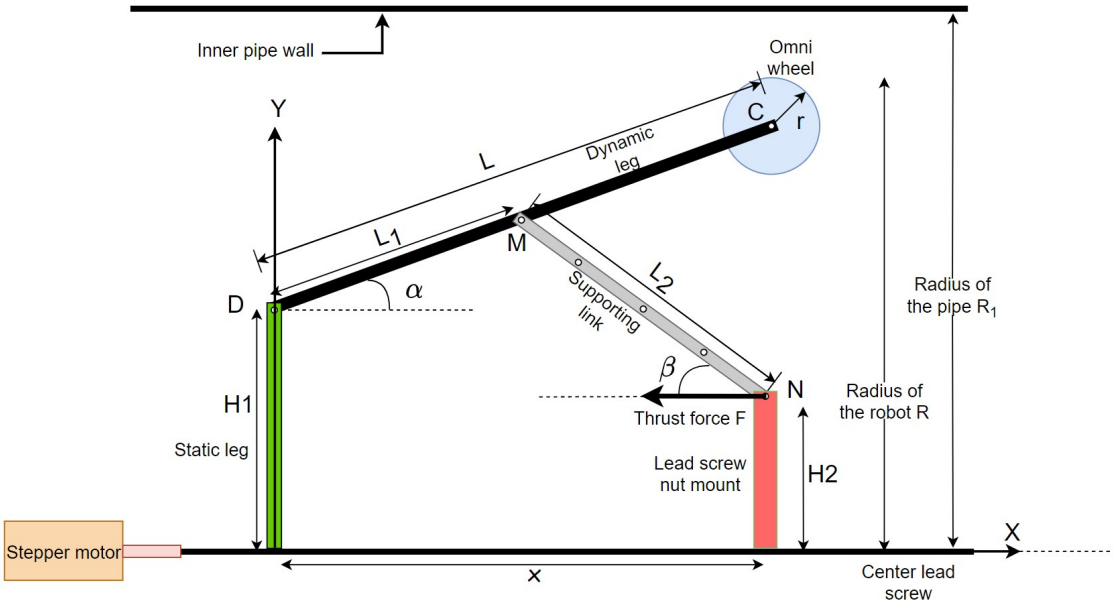

Figure 3.3: Schematics of the centering mechanism

To adapt to pipe size, the stepper motor with an output torque T produces a thrust force F which drives the linkage mechanism shown in the above figure to change the radial size of the robot, and other two sets of linkage mechanism perform same action synchronously.

At the beginning of the inspection process, the central axis of the robot does not overlap the central axis of pipe as shown in the Figure 3.4. An additional torque is required to overcome the opposition caused by the transverse friction between surface of pipe wall and the wheels supporting the gravity. This may result in over loading of the stepper motor. Therefore, analysis of this process is needed, and mechanics model to guide the design needs to be established.

The expansion and retraction of the centering mechanism is carried out when the impact-echo setup is at 0° angle in the pipe and the robot structure is symmetric around the central axis. Thus, the center of gravity, denoted by symbol G, lies at the central axis.

In the figure 3.4,

γ = attitude angle of the robot which can reflect its rotation round its central axis of a pipe;
N_1 and N_2 = supporting force acting on the two sets of a driving wheels by the gravity of the robot;
θ = is the included angle between axis OZ and the line from the supporting point of a driving wheel to the pipe center;
s = arc length of θ;
z = coordinate of G at axis OZ;
f = coefficient of transverse friction between driving wheels and pipe wall.

The geometric relationships and the equations are referred from the research paper of Zhang and Yan (2007). From the figure 3.3 and 3.4, the geometric relationships are

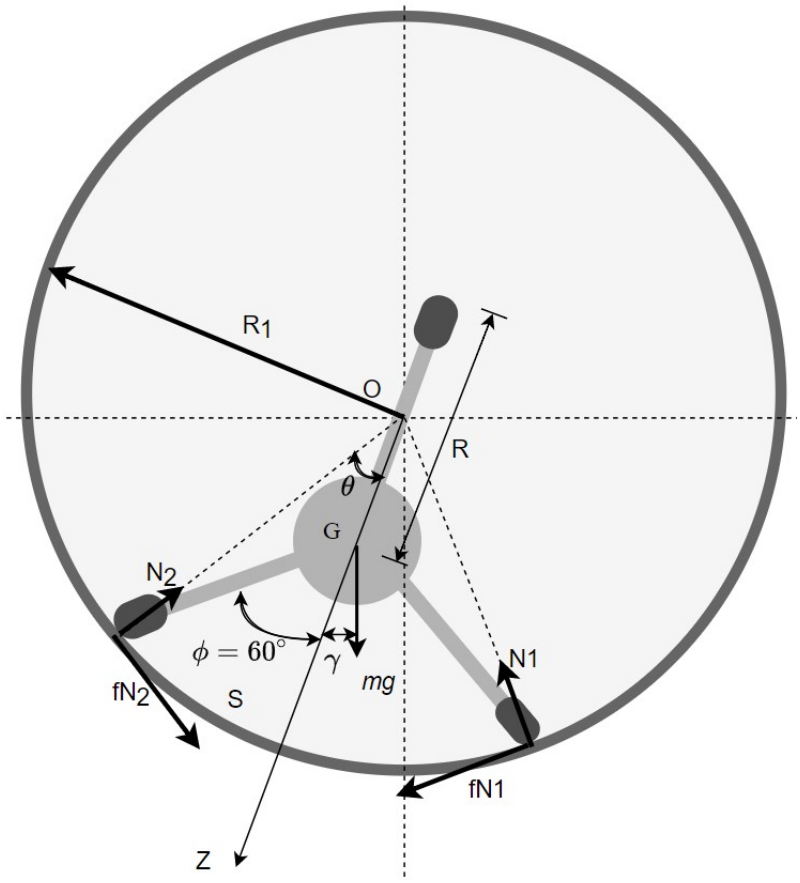

Figure 3.4: Force diagram of centering mechanism (Zhang and Yan, 2007)

$$\begin{cases} R = r + H_1 + L\sin\alpha \\ x = L_1\cos\alpha + L_2\cos\beta \\ L_1\sin\alpha = L_2\sin\beta + H_2 - H_1 \\ s = R_1\theta \\ R\sin\phi = R_1\sin\theta \\ z\sin\phi = R_1\sin(\phi+\theta) \end{cases} \tag{3.1}$$

where x is the coordinate of the point N at axis X. Differentiating both sides of equation 3.1 yields

$$\begin{cases} dx &= -\left(\frac{L_1}{L}\left(\frac{R-r-H_1}{L}\right)\sqrt{1-\left(\frac{R-r-H_1}{L}\right)^2} + \frac{1}{L}\left(\frac{-L_1(L_1(R-r-H_1)-L(H_2-H_1))}{\sqrt{L_2^2L^2-(L_1(R-r-H_1)-L(H_2-H_1))^2}}\right)\right)dR \\ ds &= \frac{R_1\sin\phi}{\sqrt{R_1^2-R^2\sin^2\phi}}dR \\ dz &= -\left(\cos\phi + \frac{R\sin^2\phi}{\sqrt{R_1^2-R^2\sin^2\phi}}\right)dR \end{cases} \tag{3.2}$$

Ignoring the frictional heating, considering a slope angle ϕ of the pipe, and according the equilibrium equation of forces and conservation of energy, following equations are obtained:

$$\begin{cases} \Sigma N = N_1 + N_2 = \frac{mg\cos\phi\cos\gamma}{\cos\theta} = \frac{mg\cos\phi\cos\gamma R_1}{\sqrt{R_1^2-R^2\sin^2\phi}} \\ Fdx + f\Sigma N ds = mfdz\cos\phi\cos\gamma \end{cases} \tag{3.3}$$

where ΣN is the sum of all supporting forces.

Defining

$$\begin{cases} k_1 &= \frac{L_1}{L}\left(\frac{R-r-H_1}{L}\right)\sqrt{1-\left(\frac{R-r-H_1}{L}\right)^2} + \frac{1}{L}\left(\frac{-L_1(L_1(R-r-H_1)-L(H_2-H_1))}{\sqrt{L_2^2L^2-(L_1(R-r-H_1)-L(H_2-H_1))^2}}\right) \\ k_2 &= \frac{R_1\sin\phi}{\sqrt{R_1^2-R^2\sin^2\phi}} \\ k_3 &= \cos\phi + \frac{R\sin^2\phi}{\sqrt{R_1^2-R^2\sin^2\phi}} \\ k_4 &= \frac{R_1}{\sqrt{R_1^2-R^2\sin^2\phi}} \end{cases} \tag{3.4}$$

and substituting equation 3.2 into equation 3.3, we get

$$F = \frac{mg\cos\phi\cos\gamma}{k_1}(k_2k_4f + k_3) \tag{3.5}$$

Then the output torque of the motor can be written as

$$T = \frac{p_h}{2\pi\eta}F \tag{3.6}$$

where η denotes the transmission efficiency of the lead screw nut pair, p_h denotes the lead of the lead screw.

The value for the variables used in the torque calculations above are shown below. These values are derived from the Solid Works model of the centering mechanism in 400 mm diameter pipe.

R = 175.86 mm
R_1 = 200 mm
H_1 = 107 mm
H_2 = 69 mm
r = 24 mm
L = 143.86 mm
L_1 = 72 mm
L_2 = 114 mm
α = 18.17°
β = 32.03°
m = 4.6 kg
g = 9.81 m/s^2

The value of γ is taken as zero from the forced diagram because in the initial configuration of the robot, OZ axis is coincident with the vertical axis. After being unsuccessful to determine the efficiency of the lead screw nut pair for this scenario, the optimum solution is to assume the value of transmission efficiency as 80%. Co-efficient of transverse friction f between the rubber roller of the omni wheel and PVC pipe is taken as 0.2 (Petrescu et al., 2017). The lead of the lead screw p_h is 8 mm.

The value of the required torque to lift the centering mechanism and center itself inside a 400 mm diameter pipe is calculated as 0.23 Nm and for a 350 mm pipe the value of required torque is 0.31 Nm.

3.2 Design of lifting mechanism

This section explains the new design of the lifting mechanism. The lifting mechanism consists of a single-stage scissor lift. Design changes are made to the base plate, top plate, and scissor links. Figure 3.5 shows the design update for the lifting mechanism.

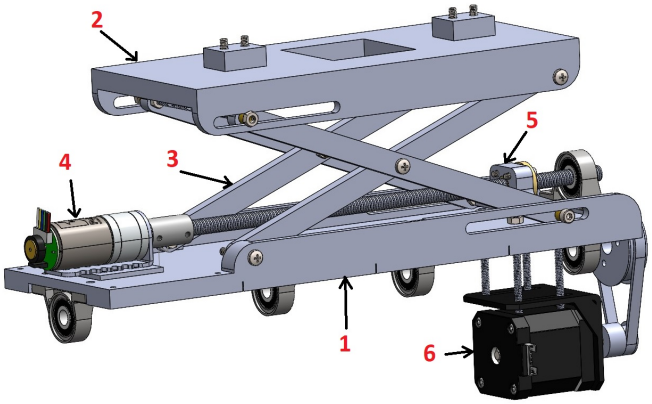

Figure 3.5: New design of the lifting mechanism
1. Base Plate, 2. Top plate, 3. Scissor links, 4. DC motor for lifting mechanism, 5. Lead screw nut mount, 6. Stepper motor for rotating mechanism

The basic structure of the lifting mechanism is not changed, but there are some changes required for the scissor links and the width of base plate and top plate. The primary reason for these changes is to reduce the mechanical play in the joints and improve the overall stability of the lifting mechanism. The width of the top plate (part 2 in Figure 3.5) and the base plate (part 1 in Figure 3.5) is increased by 20 mm to balance the weight of the lifting mechanism and the impact-echo setup when at maximum height. The width of the scissor link is also increased by 2 mm to have more contact area in the joints and reduce the tilting of the top plate while the whole mechanism is rotated. Bearings beneath the base plate are equally spaced to have better support of the base plate on the lead screw. The maximum force is required to lift the top plate when the scissor links (part 3 in Figure 3.5) are entirely closed. If the minimum angle of the scissor links with the base plate is less than 5° Ismael et al. (2019), then the lifting mechanism reaches a singular point from where a significant force is required to lift it, and it also wears the lead screw and nut. So for safety reasons, the minimum angle of the scissor links is taken as 10°. With this minimum angle, the lifting mechanism can operate in 350 mm diameter pipe size. So, the minimum operating pipe diameter is changed from 300 mm of the previous prototype to 350 mm of the new prototype. According to this minimum angle of scissor links, the slot length in the base plate and top plate are adjusted. The material of the base plate is Nylon with carbon fibre, and the top plate is ABS plastic.

3.3 Electrical Design

This section elaborates on the electric part of the design and electronics component placement. The elaboration of electronic components consists of the following topics:

- DC motor & motor driver
- Distance sensor

- Angle sensor
- Stepper motor driver
- Voltage converter for servo motor

The torque calculation required to raise the scissor lift is incorrect in the previous prototype. When raising the scissor lift from its completely retracted position, the movement of the top plate is obstructed by the lead screw nut mount. So, a new motor is required with lower shaft height and more torque. A distance sensor feedback to the lifting motor is needed, which varies the height of the scissor lift precisely. The servo motor for the impactor arm needs 6 V, so a step-down voltage converter is used, which converts the main 12 V power supply to 6 V. This servo motor is the same as the previous prototype. Keeping the same servo motor is to have precise movement control, and it is lightweight compared to the stepper motor. Another reason for not changing the 6V servo motor to 12 V is its cost. Besides, a 6 V servo motor is enough for the application. A detailed electrical circuit diagram of the new prototype is shown in Appendix F.

3.3.1 DC motor & motor driver

The torque required to raise and lower the scissor lift is calculated in Appendix B. The peak torque needed to raise the scissor lift from the completely retracted position is 0.96 Nm. The previous prototype used a 12 V stepper motor with a peak torque of 0.35 Nm, that is insufficient to raise the scissor lift. Therefore, a 12 VDC motor with a peak torque of 1 Nm is chosen. It can take up to 5 A of current, which is more than required for the lifting mechanism. The reason for selecting a DC motor over a high torque stepper motor is to reduce the overall weight of the robot. Another reason is to have a lower shaft height. The shaft height from the mounting point of the DC motor is less than the stepper motor used earlier. Lower shaft height allows the scissor lift to have enough space to retract completely without any obstruction. The lifting stepper motor used earlier weighs 600 g, including the mounting bracket. But the DC motor, including the mounting bracket, weighs around 60 g. Unlike a stepper motor, a DC motor runs continuously according to the polarity of the power supply. An H-bridge circuit is needed to control the direction of the DC motor. The L298N motor driver module is chosen to handle the motor's voltage and current. It can handle voltages in 5V - 35 V DC range and a maximum current of 2 A. It uses an H-bridge circuit to control the direction of the motor. The speed of the motor can be controlled using the enable pin of the motor driver.

3.3.2 Distance sensor

A distance sensor is used to know the distance of the impactor to the pipe wall. The distance sensor (part 1 in the Figure 3.6) gives feedback to control the DC motor. A comparison of trials of different distance sensors is shown in Appendix C. A precise distance sensor with millimeter accuracy is required to position the impact-echo setup from the pipe wall accurately. For this, the VL6180X Time-of-Flight distance is chosen. It works by emitting an infrared signal and registering its time to receive it. The range of this sensor is from 2 mm to 300 mm. It has an accuracy of 2 - 4 mm on a flat surface and a curved surface. The sensor module has high repeatability.

The placement of the distance sensor is important. It needs to be close to the impact-echo setup and in line with the impactor arm. Figure 3.6 shows the placement of the distance sensor. The distance from the steel ball (when on the magnet) to the pipe wall needs to be 40 mm, which can be adjusted later if required. The distance sensor is mounted on an extended plate at the same height on the magnet base (Figure 3.7). Even when the impact-echo setup is rotated, the sensor remains in line with the impactor arm.

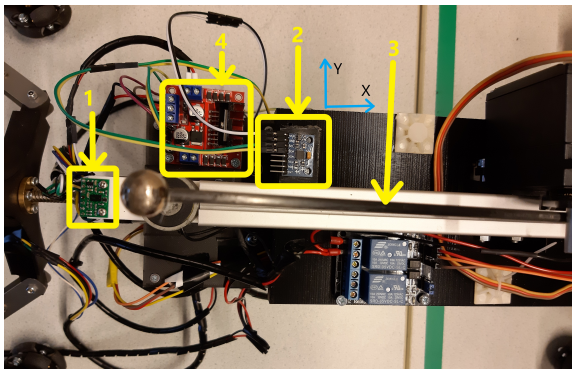

Figure 3.6: Placement of components
1. Distance sensor, 2. Angle sensor, 3. Impactor arm, 4. DC motor driver

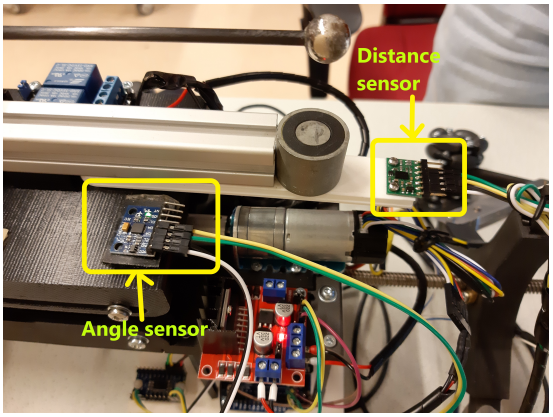

Figure 3.7: Side view of the placement of the distance sensor and angle sensor

3.3.3 Angle sensor

The mechanism is rotated about the base plate to orient the impact test setup inside the pipe. An angle sensor is used to know the angle at which the impact is made. The sensor used here is MPU-6050, consisting of a 3-axis accelerometer and a 3-axis gyroscope. It is the same sensor used in the previous prototype for homing the rotating mechanism. As the impactor test setup is mounted on the top plate, the angle sensor is also mounted on the top plate, as it can be seen in Figure 3.7. The top plate and base plate remain parallel when the impact-echo setup is upright. But as soon as the impact-echo setup starts to rotate, the top plate and base plate do not remain parallel. It is because of the tilting of the top plate. The tilt happens due to some mechanical play in the scissor lift mechanism and the weight of the impact-echo setup. Thus, the angle sensor is placed on the top plate to know the correct angle of the impact-echo setup. From the orientation of the MPU-6050 sensor, the roll angle must be calculated from the sensor data. The output of this sensor does not directly provide the roll angle. So, to find the roll angle, the accelerometer data of the sensor is required. The 3-axis accelerometer measures the linear acceleration of a body on each axis. The calculation of roll angle from the acceleration data is given below Fisher (2010):

$$roll\ \ angle\ \ \theta = \tan^{-1}\left(\frac{Accel_x}{\sqrt{Accel_Y^2 + Accel_z^2}}\right) \times 180/\pi \tag{3.7}$$

where, $Accel_x$, $Accel_y$ and $Accel_z$ are the linear acceleration along X, Y and Z axis.

3.3.4 Stepper Motor driver

The previous prototype had the TB6600 stepper motor driver to control the stepper motor. These modules are extensive in size, and thus they are placed in an electronic box separate from the robot. A compact alternative was needed to be implemented on the new prototype to optimize the electronics and make it portable. The stepper motor driver used in the new prototype is a dual stepper motor driver shield (DRV8825) which can be directly mounted on the Arduino. This motor driver shield controls the steering and rotating stepper motor. The driver shield is directly mounted on the Arduino MEGA ADK. The driver shield consists of push spring connectors, which makes the stepper motor reliable.

The direction of rotation for the centering and rotating stepper motor is controlled by setting the direction signal to LOW of HIGH. The stepper motor has a 1.8° step angle, which means 200 steps complete the revolution. It is considered the full-step mode. But the stepper motor

can be set to various micro-step resolutions using the stepper motor driver. 1/2 (half mode), 1/4 (quarter mode), 1/8, 1/16, and 1/32 modes are available. Both the stepper motors are set to 1/8 micro-step mode. That means there are 1600 micro-steps in a revolution. A pulse signal is provided to the stepper motor to change the step angle.

3.3.5 Voltage converter for servo motor

The operating voltage for the servo motor is 5 - 6 V. So, it can work on Arduino's 5V power. Still, the motor's torque is not enough to move the impactor arm to the magnet because there is a rotational spring attached to the impactor arm. Therefore, more power is required. With a 6 V power supply, the torque generated by the motor is enough to put the impactor arm of the servo motor to the magnet. The main power supply of 12 V is stepped down to 6 V using an LM2596 buck converter. This module can take input voltage from 4V - 35 V DC and provides output in the range of 1.23 V - 30 V. It can handle up to 3A peak current.

3.3.6 Electronics Component placement

The electronic components are placed on the robot to get more portability. A power cable, Arduino cable, and Logitech gamepad controller cable comes out of the robot. An on/off switch is provided within the power cable. A hanging platform below the base plate is used to mount all components except the DC motor driver. The platform contains the Arduino MEGA ADK, dual stepper motor driver shield, buck converter, and I2C multiplexer. The DC motor driver (figure 3.7) is mounted on the base plate just beside the DC motor to minimize the wiring. The I2C multiplexer is used to communicate two sensors with the Arduino. The height of the platform is also such that it does not hinder the rotation movement of the mechanism.

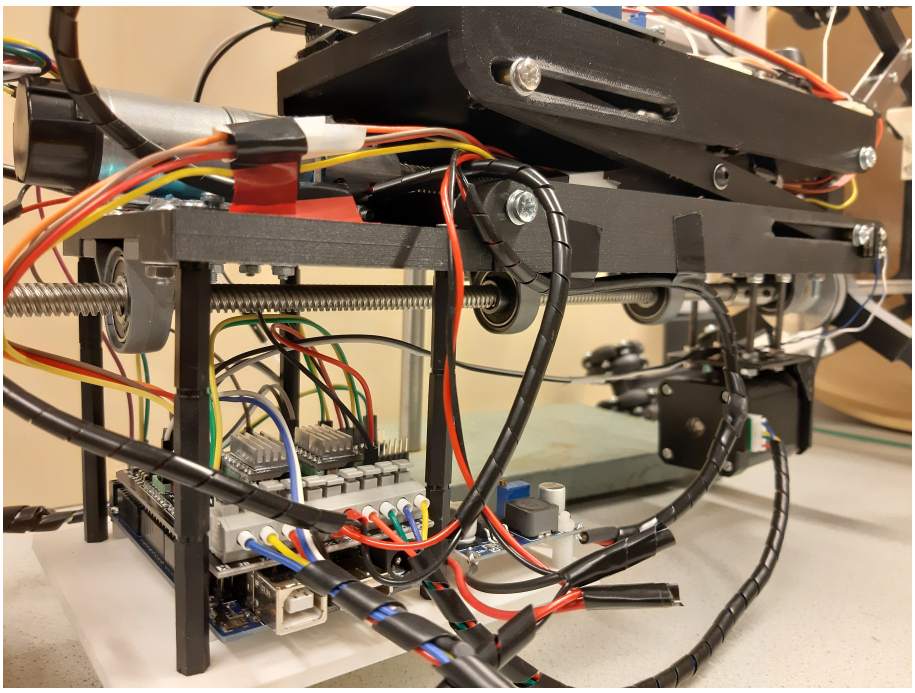

Figure 3.8: Electronics Component re-arrangement

3.4 Controller Design

This section includes the control method used for the lifting mechanism and rotating mechanism and elaboration of the control routine of the working procedure. Manual control routine is already used in the previous prototype and is explained in Chapter 2. Every task is assigned a button on the Logitech gamepad controller in a manual control routine. Now, a semi-

automatic control routine is developed for the new prototype. Some of the tasks are automated using sensor feedback, and pre-calculated step counts for the stepper motor in this control routine. Some of the tasks still need manual input from the Logitech gamepad controller.

A block diagram of the control system for the lifting mechanism and rotating mechanism is shown in Figure 3.9 and 3.10 respectively.

A feedback controller is implemented for the lifting mechanism. The controller sets the reference distance between the impact ball and the impact point (pipe wall). The reference and actual distances are compared, and the signal is provided to the L298N motor driver. As soon as the error goes to zero, the controller sends a command to stop the motor and thus stop the desired height of the scissor lift mechanism is achieved. The Time-of-Flight distance sensor is used to control the motion lifting mechanism. A model-specific library for the sensor is used in Arduino to get readings from the sensor. The sensor output is in the form of distance in millimeters. This distance is directly used as feedback to control a DC motor. A while loop is used to monitor the distance data from the sensor continuously.

For control of the rotating mechanism, a P controller is used. A reference angle is provided to the controller. This reference angle is the desired angle of impact inside the pipe. The MPU-6050 sensor module is used to control the angle of the mechanism. The sensor is mounted on the top plate where the impact-echo setup lies. The rotation stepper motor rotates the base plate. As the base plate and the top plate are parallel, both will be at the same angle when rotated. This sensor module provides the acceleration data along all three axes, and then the roll angle is calculated from it. The rotating mechanism rotates about the robot's central axis, which is the X-axis of the sensor based on its orientation. So, rotation about X-axis is the roll angle. The equation used to find the roll angle is given in the equation 3.7. Then the difference of reference angle and measured angle is fed to the controller. It is multiplied by a gain value, and required step counts are obtained. The calculation to obtain step counts is shown in Appendix E. The stepper motor is operated based on this step count. After completing the initial rotation command, the control loop runs again to check the error and sends the required step counts to the stepper motor based on overshoot or undershoot.

The initial input to start the control loop is taken from the Logitech game controller, and the readings are monitored on the Arduino's serial monitor. Arduino is the primary controller that processes the control logic and sends necessary commands to the motor driver and the motors. Sensors and the limit switches send feedback to the Arduino, which controls the motor output to get desired results.

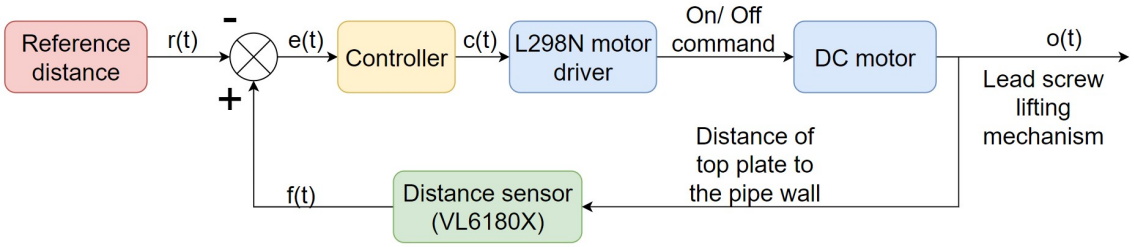

Figure 3.9: Block diagram of position control of lifting mechanism

3.4.1 Semi-Automatic control routine

Apart from the manual control routine (Figure 2.7), a semi-automatic control routine is also developed to automate the inspection procedure and reduce human errors. An Arduino MEGA ADK controller controls the inspection robot. The control code of the inspection robot is developed in Arduino IDE software. A Logitech gaming controller is used to give commands wherever required. The gaming controller is directly connected via a USB cable to the Arduino.

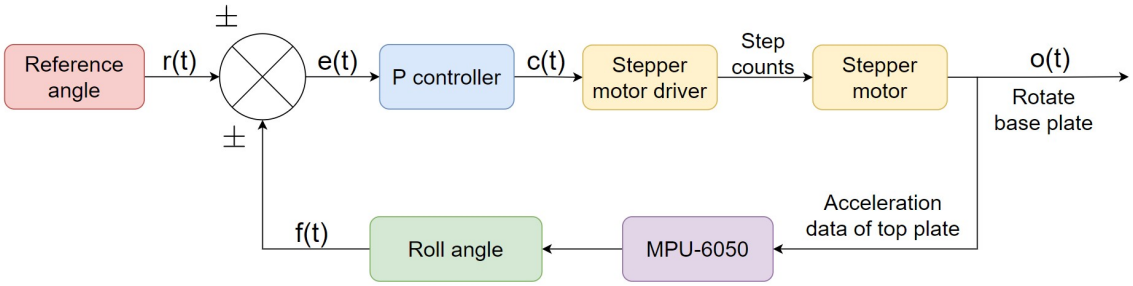

Figure 3.10: Block diagram of angle control of rotating mechanism

Arduino senses which button is pressed and runs a block of code corresponding to it. More information on which button is responsible for giving which command is provided in Appendix D. The impact test procedure is shown in Figure 3.11. The flowchart showing the semi-control routine is shown in Figure 3.12.

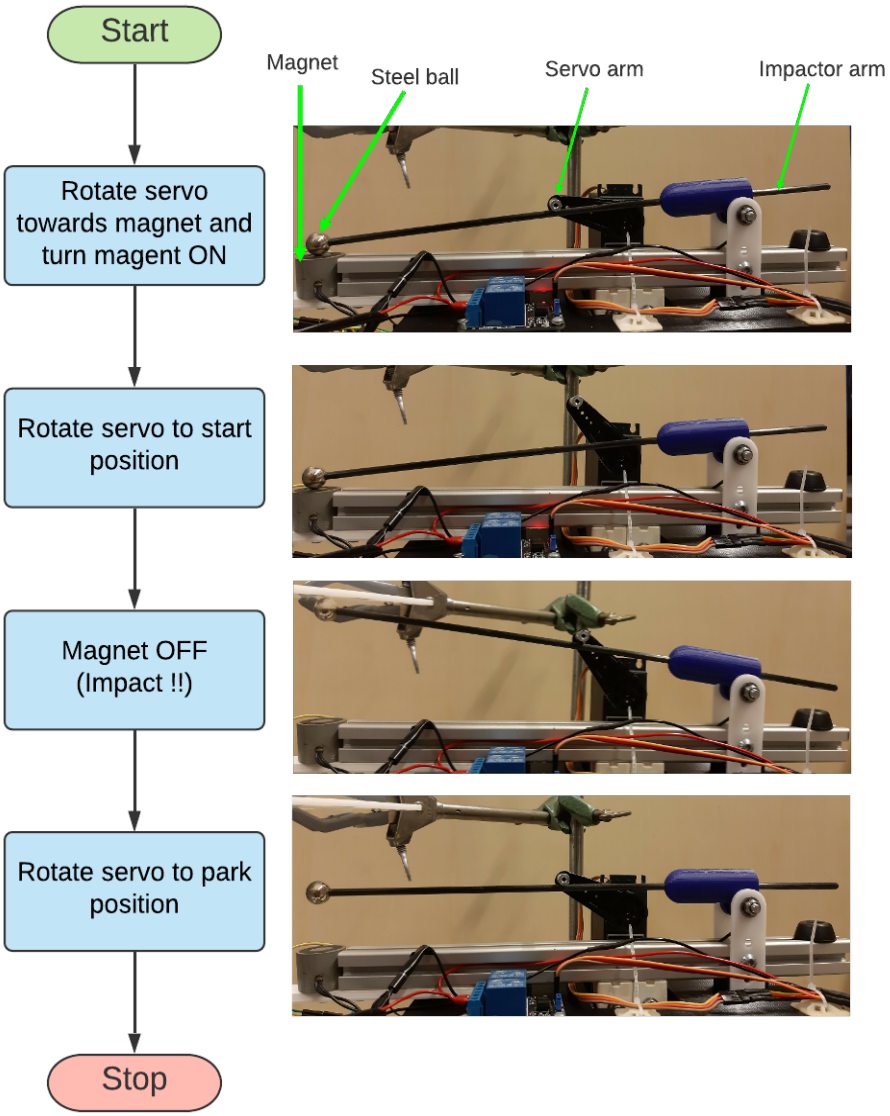

Figure 3.11: Impact-echo test procedure

The semi-automatic control routine is divided into eight states. A brief description of each state is provided in the flowchart. These states are programmed with switch-case statements.

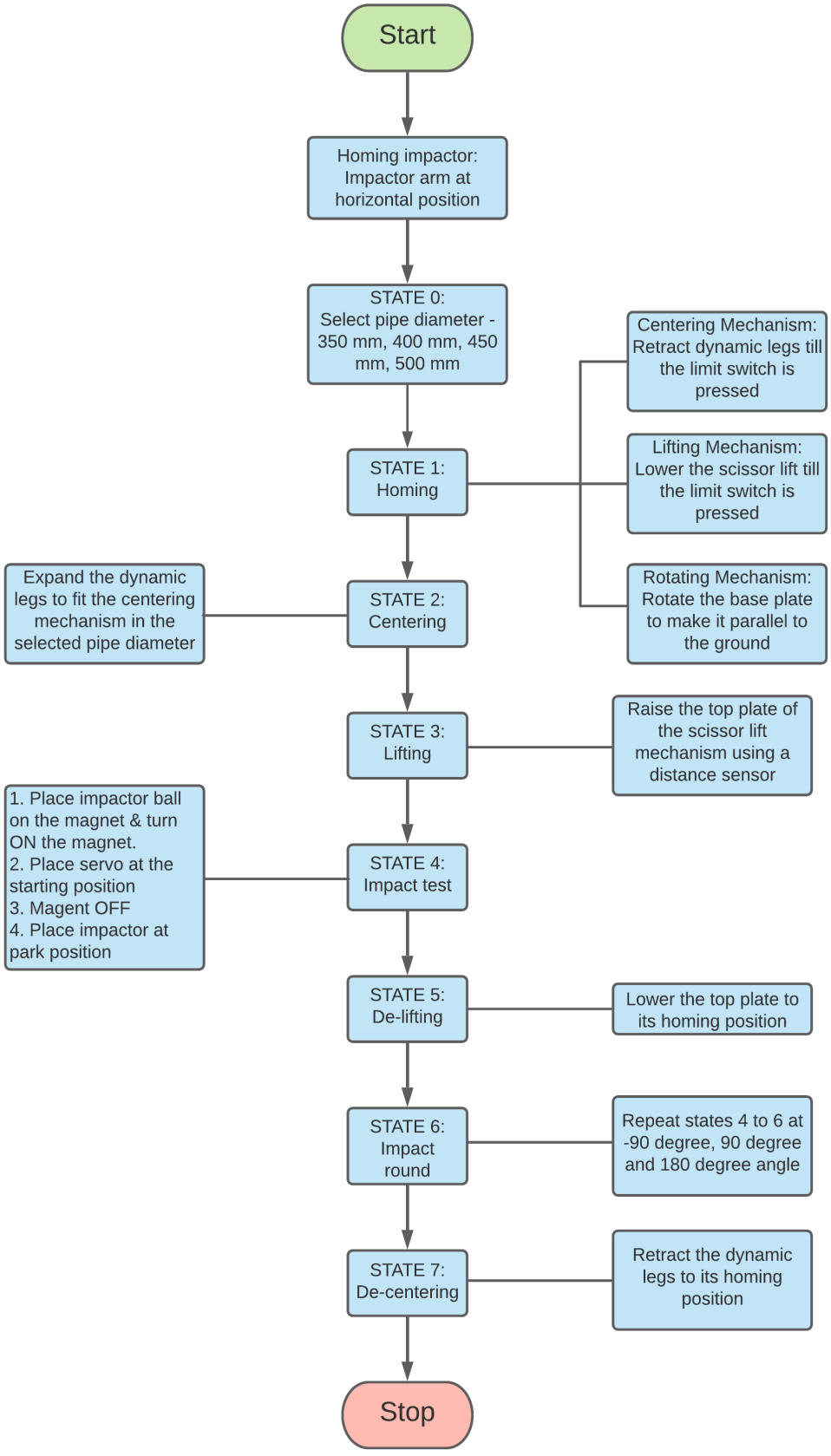

Figure 3.12: Semi-automatic routine

Manual control input is required for every state to start. The details of tasks assigned to different buttons at different states are given in Appendix D. After receiving the command, tasks set for the particular state are automatically performed.

State 0 includes the pipe diameter selection. Four pipe sizes can be chosen from 350 mm, 400 mm, 450 mm, and 500 mm. Four different buttons are assigned to select for each pipe size. After selecting the pipe size, the algorithm switches to state 1.

In state 1, homing of all three mechanisms is performed. Homing of the centering mechanism, lifting mechanism, and rotating mechanism is described in the flowchart. The control algorithm then carries out all homing procedures. After completion of homing, the control algorithm shifts to state 2, in which centering is performed.

In state 2, the centering stepper motor runs for a pre-calculated number of steps based on the pipe size chosen in state 0. The calculations of the steps needed to expand the dynamic legs and adapt the pipe size are shown in Appendix E. There is no feedback control for this task.

State 3 is lifting. In the lifting state, the impact-echo setup platform is raised to the height from where the impact distance is about 4 cm. As soon as lifting action starts, the distance sensor is activated, and continuous distance readings are monitored. The lifting motor stops as soon as the desired height is reached. Here, a proportional control method is used to control the height of the platform.

State 4 is the impact test. The procedure of the impact test is shown in Figure 3.11. A delay of 1 second is kept between every step of the impact-echo test procedure.

State 5 is de-lifting. This state lowers the impactor platform till the lifting mechanism reaches its homing position. It completes the impact test at the top of the pipe, which is considered as 0° angle.

State 6 is impact round. In this state, the impact echo test is performed at three other points on the circumference of the pipe. The rotation mechanism rotates the base plate about the center lead screw. So, first, the impact echo test is performed at -90° angle and then at 90° and 180°. More angles can be added to have more impact points by changing the code. The required step count for the rotating stepper motor is calculated based on the angle data. This calculation is shown in Appendix E. This sequence is chosen so that the cables running through the robot do not get entangled with each other. For this thesis, only these four distinct points are selected to inspect a particular section of the pipe to check the performance of the control method used for it. Impact echo test can be performed at any desired angle in the pipe if required. States from 3 to 5 need to be run after setting the impact test setup at a particular angle.

In state 7, de-centering is performed in which the centering mechanism is put back to its homing position. It marks the completion of inspecting a section of the pipe.

This working procedure inspects a particular section of the sewer pipe. After de-centering, the robot is moved further into the pipe to inspect the next area. So, for every pipe section to be checked, the centering and de-centering of the robot are required.

Figure 3.13 and 3.14 shows the front view and the side view of the complete integrated prototype model in Solid Works.

This chapter concludes that the design of the centering mechanism and lifting mechanism is made to improve the limitations of this pipe inspection robot's previous prototype and requirements. Also, a semi-automatic control algorithm is developed to automate the inspection procedure. The electronic components are re-arranged and replaced to make it compact and make the robot portable to transport. The following chapter discusses the experimental setup and results for this new prototype.

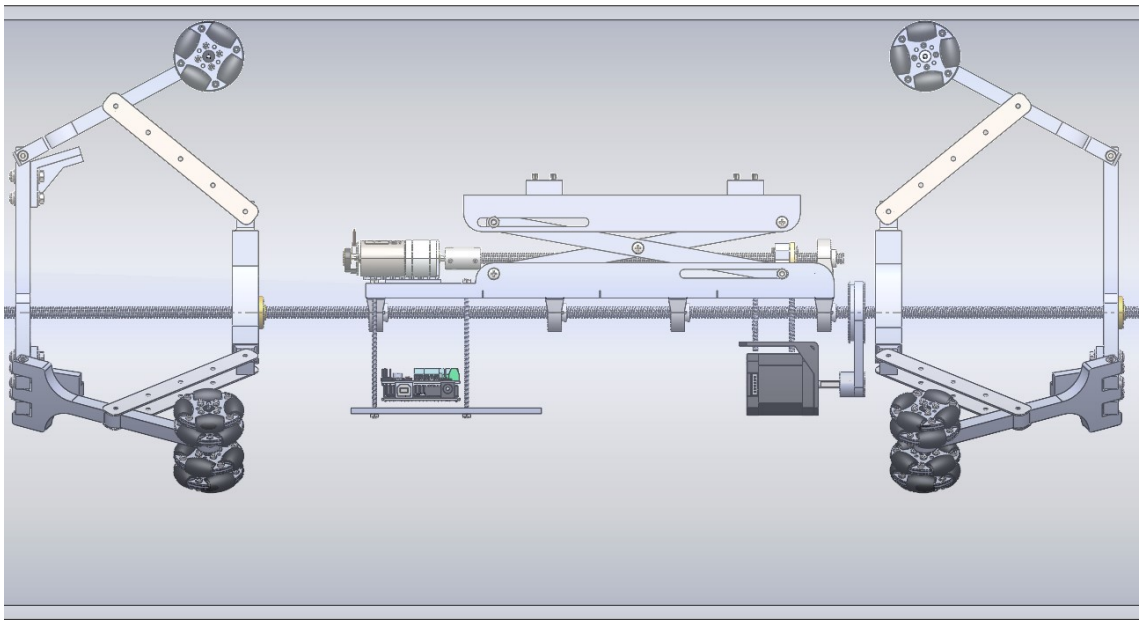

Figure 3.13: Complete model of new prototype in Solid Works Front view

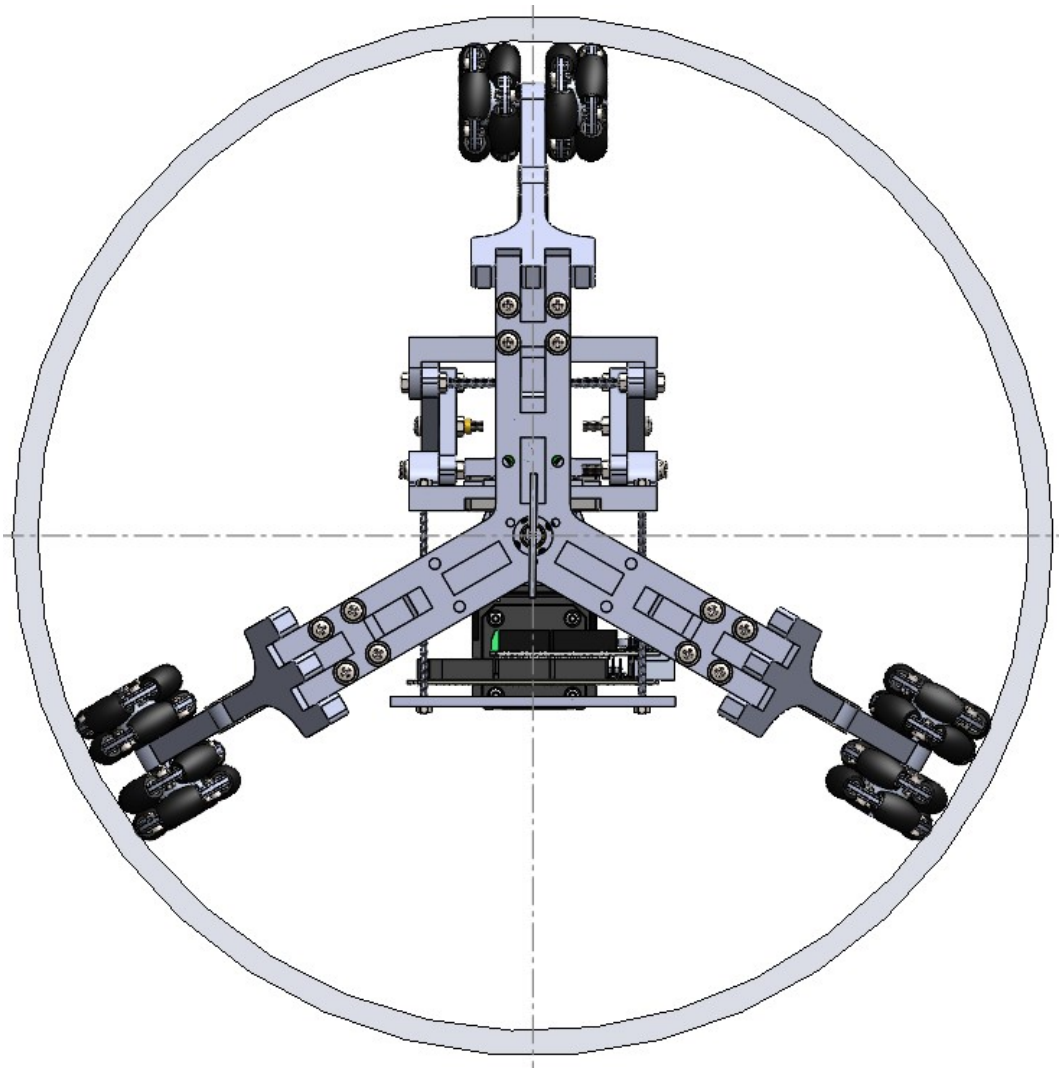

Figure 3.14: Complete model of new prototype in Solid Works Side view

4 Experiments and Results

This chapter discusses the testing and evaluation of the centering, lifting, and rotating mechanisms individually. The assessment of the centering mechanism is done based on its ability to center the robot inside the pipe. The lifting mechanism is evaluated based on the precision of the distance sensor and the control method's reliability. The rotating mechanism is assessed based on the performance of the angle sensor and the feedback control algorithm used for the rotation. At last, the performance of the whole robot is evaluated based on the requirements mentioned in chapter 2.

4.1 Centering mechanism test

4.1.1 Test setup

This section briefs the experiments performed for the centering mechanism and its ability to perform inside the pipe. The experimental setup for testing the centering mechanism is done by putting the entire robot inside the pipe and operating just the centering mechanism. The experiment is performed in a 400 mm diameter PVC pipe.

The testing procedure includes expanding the centering mechanism with manual control (open-loop control) of the stepper motor to fit inside the 400 mm pipe. The observations to be made are if the centering mechanism can lift the whole robot inside the pipe and align the central axis of the robot with the pipe center. The test setup is shown in the Figure 4.1.

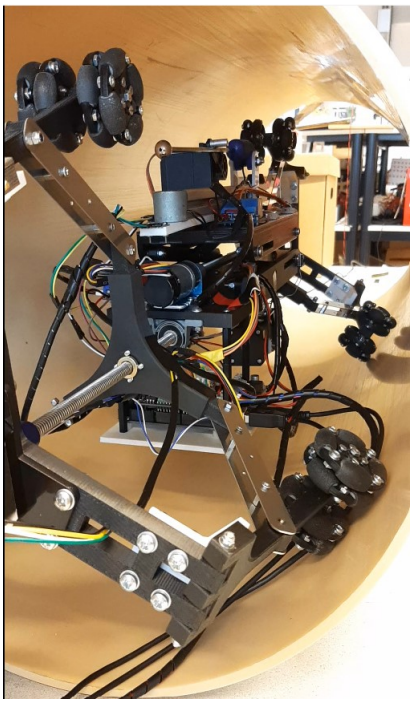

Figure 4.1: Experimental setup of the centering mechanism design 2 inside a 400 mm pipe

4.1.2 Results and discussion

As the test is performed using manual control, there are no readings to show. So, the results for the centering mechanism are mainly based on observations. The results of this test show that the performance of the centering mechanism is improved compared to the previous prototype. The rolling friction between the Omni wheels and the pipe wall is less than the sliding friction of the wheels in the previous design, and therefore the dynamic legs can expand freely inside

the pipe. The centering mechanism can lift the robot and expand the leg structure inside the pipe, but it can still completely adapt inside the 400 mm pipe. The mechanism gets stuck after expanding up to a certain point. It gets short by a few millimeters (see figure 4.2) to completely fit inside the 400 mm pipe. The maximum required torque by the centering stepper motor is when the robot is in 350 mm pipe, which is 0.31 Nm. The rated peak torque of the centering motor is 0.73 Nm. So, in theory, it is sufficient. But the exact reason why complete centering is not achieved is unknown. It can be concluded from this test that the centering mechanism works partially and does not achieve the goal of adapting the robot inside the pipe completely.

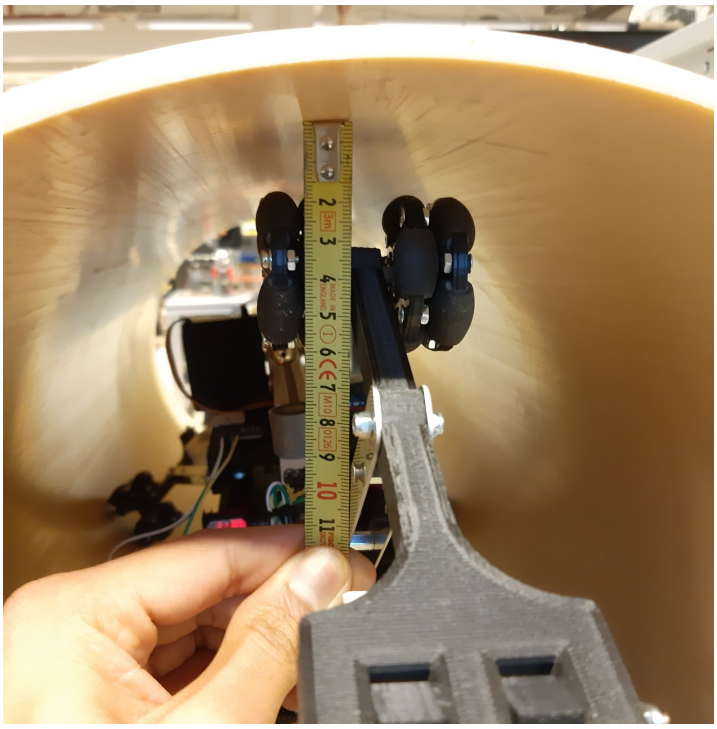

Figure 4.2: Results of centering mechanism showing a gap of 15 mm to completely fit inside the pipe

4.2 Lifting mechanism test

4.2.1 Test setup

The test of the lifting mechanism is performed in the same 400 mm PVC pipe. The test setup is also the same. As the test is only for the lifting mechanism, a separate code is executed to perform lifting and de-lifting of the scissor lift based on the feedback from the distance sensor. Figure 4.3 and 4.4 shows the lifting mechanism at homing position and at top position. The test procedure is that the scissor lift starts raising by pressing a button on the game controller and stops automatically at a set distance. Another button is pressed to put back the scissor lift to its homing position. The same buttons are used here as in the semi-automatic control routine. This test procedure is repeated a certain number of times to check the repeatability of the sensor.

This test aims to check the performance of the lifting mechanism with the newly installed distance sensor and DC motor. The set value for the distance sensor is given as 70 mm, considering its mounted level. The height of the magnet is about 25 mm. The impact distance is calculated from the center of the steel ball to the pipe wall. It needs to be 40 mm.

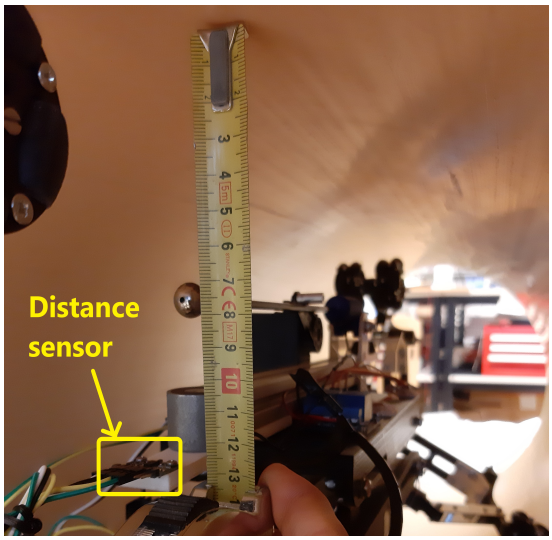

Figure 4.3: Lifting mechanism at homing position

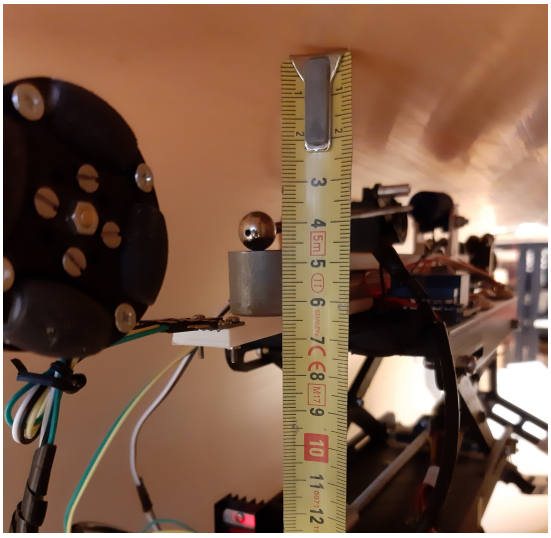

Figure 4.4: Lifting mechanism at the desired distance from the pipe wall

4.2.2 Results and discussion

Figure 4.3 and 4.4 shows the before and after states of the lifting mechanism when lifting task is performed. Initially, the lifting mechanism is at its homing position with a distance from the distance sensor to the pipe wall of 130 mm. After the lifting is complete, the distance from the distance sensor to the pipe wall is 70 mm. It can also be seen from the figure 4.4 that the distance from the steel ball to the pipe wall is 40 mm. Thus, the control algorithm for the lifting mechanism is working as expected. The lifting and de-lifting tasks are carried out multiple times to check the repeatability and reliability of the system. Figure 4.5 shows the test results in the serial plotter of the Arduino. Y-axis represents the distance in mm, and X-axis represents the number of times the execution of print commands. The red line represents the distance sensor readings. It can be seen that when the scissor lift is at the home position, the distance from the sensor to the pipe wall is around 130 mm, and the scissor lift stops when it reaches 70 mm distance. Then, the scissor lift is brought back to its homing position. This is considered as one cycle. The graph shows tests results of 6 cycles of the same. The tests are done keeping the impact-echo setup at 0°, i.e., impact on top. The average of 6 cycle readings, where the scissor lift stops, is 68.5 mm. The difference of 1.5 mm is noticed because it is programmed to stop if the reading of the sensor goes below 70 mm. When the actual measurement of the distance was done for every cycle, then it was seen that it stops at 70 mm precisely. Thus, the readings are consistent, and the sensor's repeatability is also sufficient to perform the impact-echo test.

A problem is also encountered with the sensor. A difference of 5 mm to 10 mm in the sensor readings on Arduino's COM port and the actual distance is noted. This is better visualized in the Figure 4.6 and 4.7. Figure 4.6 shows that the lifting mechanism starts at a distance of 93 mm and it stops at a 70 mm distance. But comparing this reading with the actual distance, it can be seen from Figure 4.7 that the distance from the sensor to the top white plate is 75 mm. So, an offset of 5 mm is noted. This offset is not observed every time, but it appears randomly and goes off after restarting the system. This behaviour is not known exactly because the same behaviour was noticed with another VL6180X sensor module.

Another problem is with Arduino's serial monitor. Randomly the serial monitor stops working and thus giving erroneous results. A simple solution for both these problems is to restart the serial monitor or restart the Arduino IDE software. But this is not the permanent solution for this problem. Maybe a different kind of distance sensor solves the offset problem.

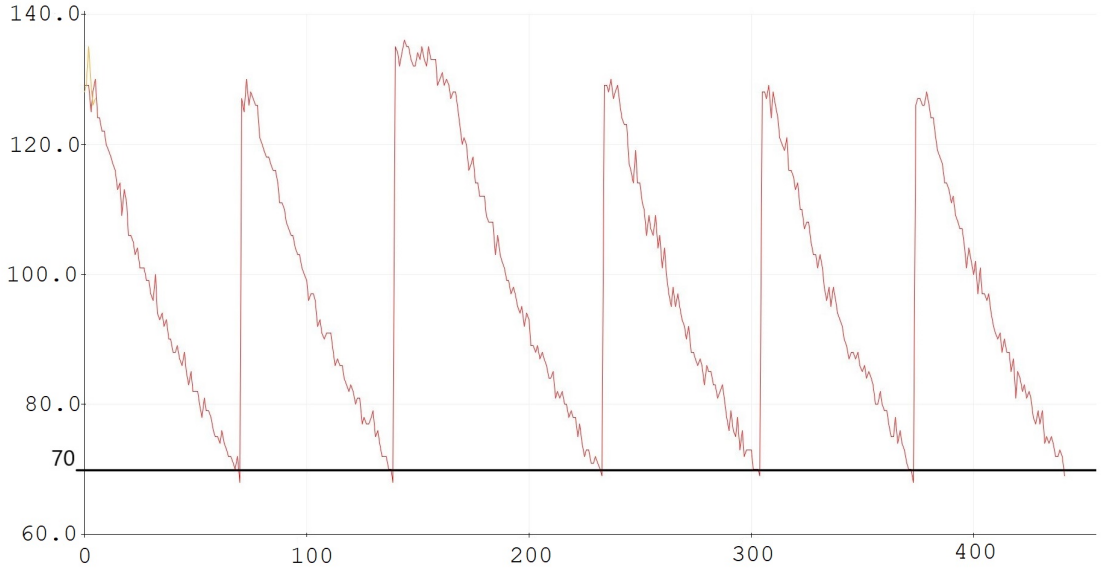

Figure 4.5: Lifting mechanism test results in the serial plotter of Arduino

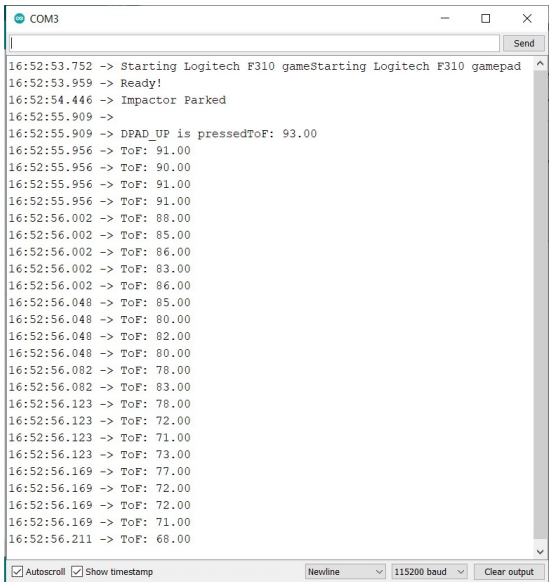

Figure 4.6: Actual distance from the sensor to the white plate

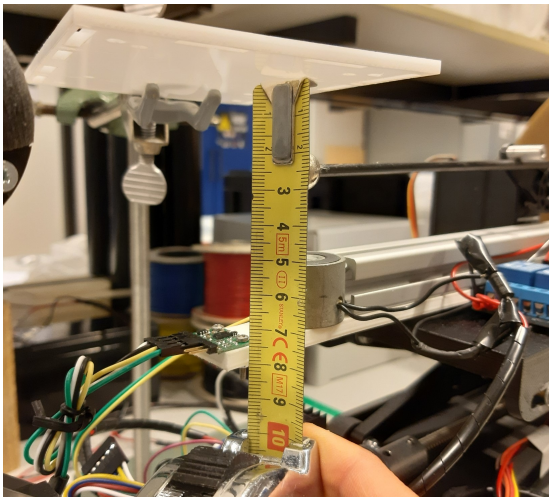

Figure 4.7: Distance sensor readings on Arduino's serial COM port

4.3 Rotation mechanism test

4.3.1 Test setup

The test setup for the rotation mechanism is kept the same as the lifting mechanism and centering mechanism. The testing of the rotation mechanism is performed independently by executing a separate code. This test aims to check the performance of the rotation mechanism using the angle feedback from the MPU-6050 sensor module. The impact-echo setup is rotated to $-90°$, $90°$ and $180°$ in an irregular fashion. It is done to check the precision of the feedback controller for the rotating mechanism. Figure 4.8, 4.9 and 4.10 shows the Rotation mechanism at $-90°$, $90°$ and $180°$ respectively.

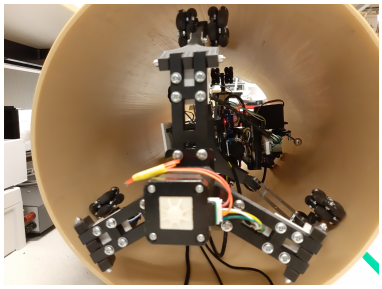

Figure 4.8: Rotation mechanism at −90° angle (impact on right)

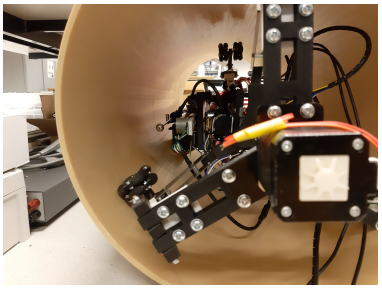

Figure 4.9: Rotation mechanism at 90° angle (impact on left)

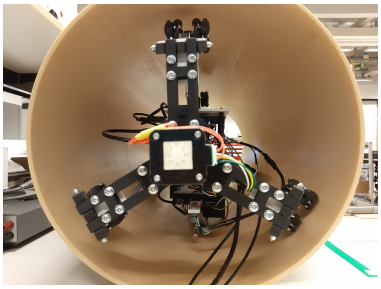

Figure 4.10: Rotation mechanism at 180° angle (impact at bottom)

4.3.2 Results and discussion

The results of the test are recorded in Arduino's serial COM port and are shown in Figure 4.11. Initially, the rotation mechanism is at 0° angle. Then, it is rotated by 90° to impact on the right side and then to the left side and then to the bottom, and then finally homing is done. As soon as the command to rotate is given, the control algorithm shows the initial angle. Then it shows the intermediate angle after completing the initial rotation, and then the control algorithm corrects the angle if needed and prints the final rotation angle. Figure 4.12 shows the same results in Arduino's serial plotter. the yellow vertical lines indicate the rotation from one angle to another, and the flat lines indicate that the set angle is achieved. The correction of the angle done by the control algorithm is not visible in the image. This same procedure is repeated for every other angle. There is undershoot or overshoot of the rotation mechanism after its initial rotation. The reason for this is that the location of the MPU-6050 sensor. The calculation of the required step count for the rotation stepper motor is done considering that the sensor is close to the rotation axis. But it is mounted at a distance from the rotation axis. The calculation for this case is not done because it involves uncertainty of the tilting of the top plate when the mechanism is rotated (clockwise or counter-clockwise). The titling happens due to mechanical play in the lifting mechanism. So, this introduces some errors in the actual step count. Thus, it requires correction in the angle achieved by initial rotation because the base plate and the top plate are not parallel anymore. As the sensor is mounted on the top plate, the resulting angle either undershoots or overshoots the set angle by 1 - 3 degrees. The reason for mounting the sensor on the top plate is that the impact test setup is also mounted on the top plate, and that is why measuring the angle of the top plate makes the placement of the impact test setup accurate.

It can be concluded that the robot can perform an impact echo test precisely at four distinct locations inside the pipe using the feedback control. There was no close loop control for the rotating mechanism in the previous prototype. Further, if required, by changing the control algorithm, an impact echo test can be made at multiple angles apart from these four angles.

4.4 Complete robot test

4.4.1 Test in 400 mm PVC pipe

After performing tests of individual mechanisms, the test of the integrated new prototype is done inside the same 400 mm PVC pipe. The semi-automatic control routine is followed for this test. The whole robot is placed inside the pipe keeping the 12 V battery and the game controller outside. The complete new prototype is shown in the Figure 4.13. The test setup of the new prototype inside the pipe is shown in Figure 4.14.

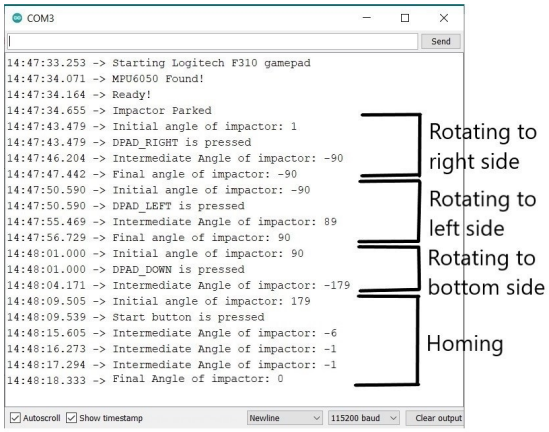

Figure 4.11: Rotating mechanism test results in the serial COM port of Arduino

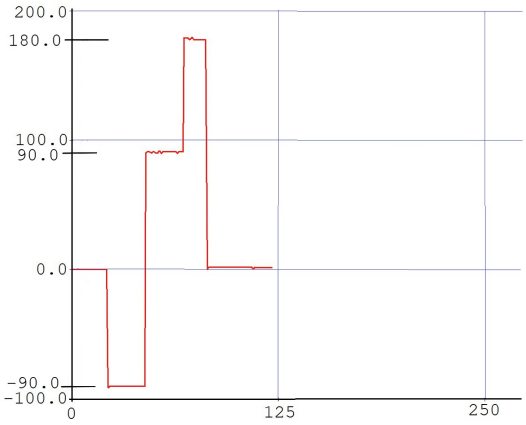

Figure 4.12: Rotating mechanism test results in the serial plotter of Arduino

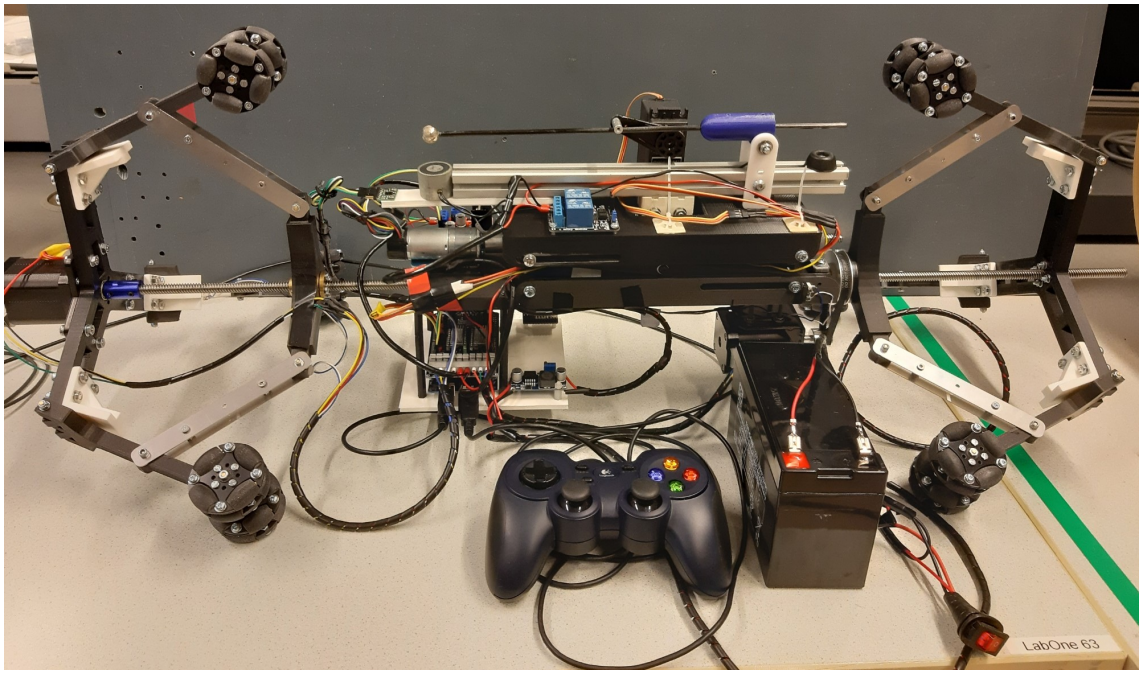

Figure 4.13: Complete new prototype

Results

The test results are recorded in the Arduino's serial COM port, and a video is made simultaneously. The main observations of the test are listed below:

- The centering mechanism works partially. It needs to be manually lifted by hand to achieve the stepper motor's last couple of step count.
- After centering is complete, the mechanism can hold the robot inside the pipe until the end of inspection without any slip.
- The scissor lift can stop at the set distance from the pipe wall for the impact test conducted at every angle.
- The impact-echo test is performed the same way as the automatic test procedure mentioned. There are no other disturbances at the time of impact, apart from a light humming sound of the rotation stepper motor.

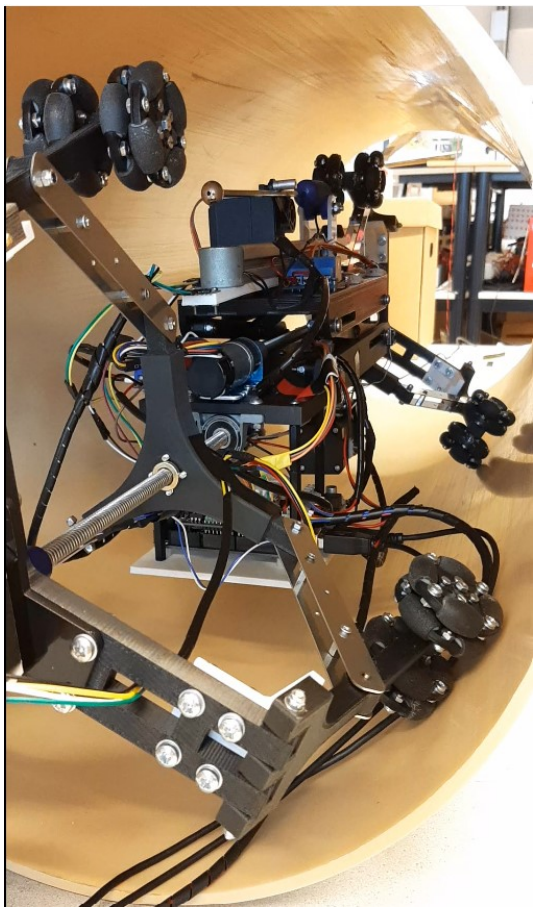

Figure 4.14: Test setup for the new prototype of pipe inspection robot

- The rotation mechanism can place the impact test platform at the set angles programmed in the control algorithm with a minor error.

The overall run time of the test is 2 minutes. The images shown in Figure 4.19 is the sequence in which the prototype performs the impact test on a section of the pipe. The robot needs to be pushed or pulled inside the pipe to perform the next section of the pipe. This task is done manually, but the crawler robot, as mentioned in Chapter 1 and shown in Figure 4.20, can be attached to the new prototype to perform this task. The crawler robot consists of a camera module mounted at one end of it through which visual inspection of the pipe can be carried out.

4.4.2 Testing in the concrete pipe

An experiment of the new prototype was also done in the concrete pipe. The condition of the concrete pipe is clean from the inside (like new). The purpose of this test is to check the robot's performance in a concrete pipe and identify cracks in the pipe structure and voids around it. The diameter of the pipe is 400 mm. The test site and the test setup is shown in the Figure 4.21 and 4.22 respectively.

Results

Observations made in the test are that the centering mechanism does not work in the concrete pipe because of the high friction between Omni wheels and pipe wall. This type of Omni wheel is not suitable for the smooth expansion of dynamic legs inside the concrete pipe. An Omni wheel with several rollers placed closely to each other might solve this problem. So, to perform

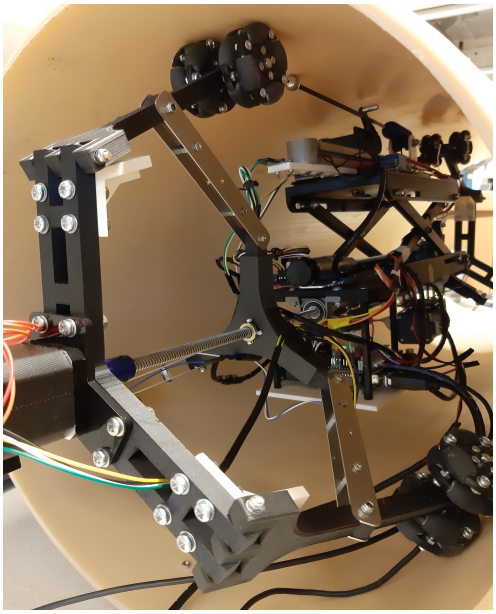

Figure 4.15: Impact at top

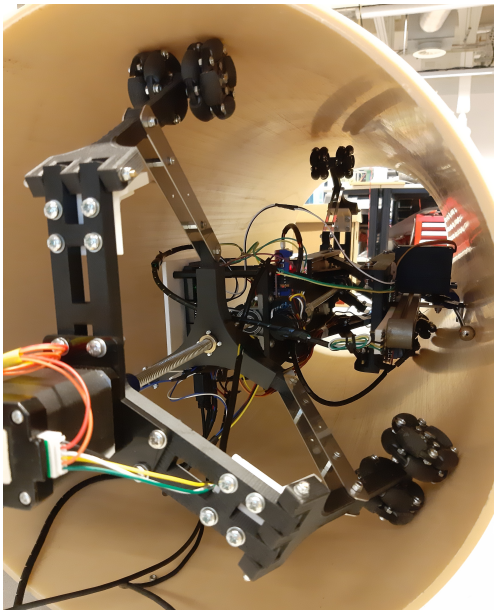

Figure 4.16: Impact on right

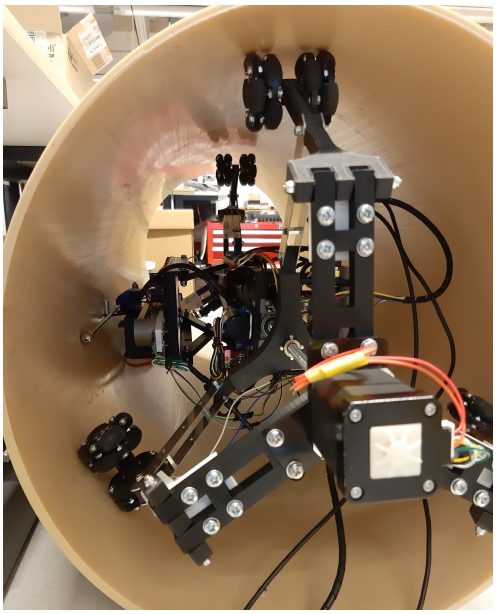

Figure 4.17: Impact on left

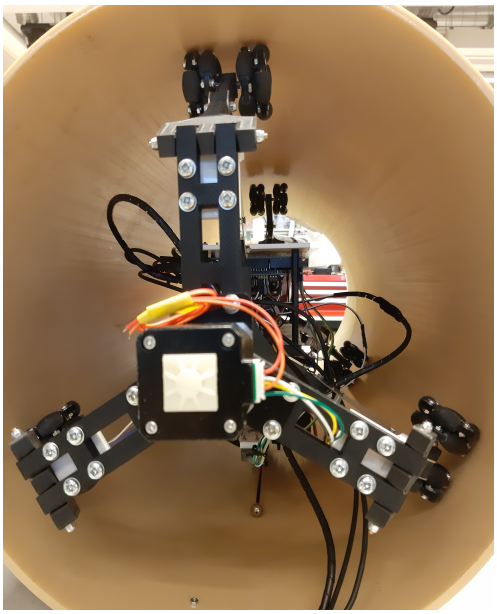

Figure 4.18: Impact at bottom

Figure 4.19: Impact at different location inside the 400 mm pipe

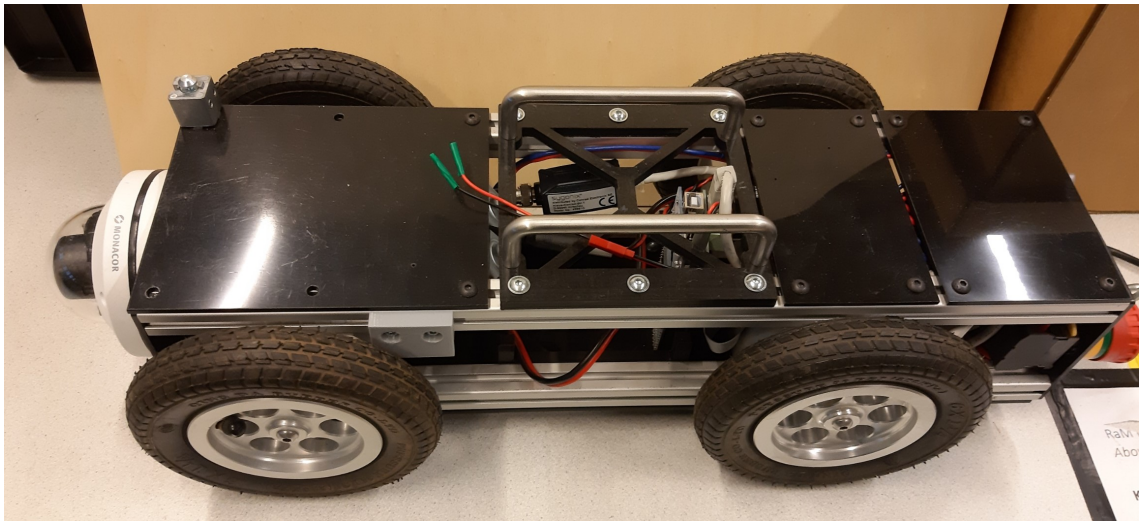

Figure 4.20: Wheeled robot to push or pull the inspection robot inside the sewer pipe

Figure 4.21: Test site for concrete pipe

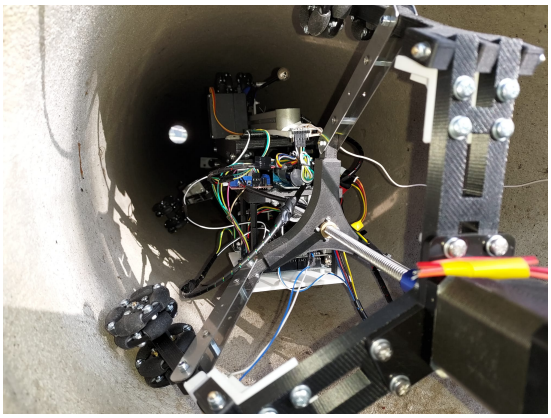

Figure 4.22: Test setup in the concrete pipe

the test, the robot was lifted by hand to fit inside the pipe. Apart from the centering mechanism, all other mechanisms work successfully. The performance of the distance sensor was the same as in the PVC pipe, even after considering the rough and uneven surface of the concrete pipe. For this test, the semi-automatic control routine is followed. Portability of the robot helped transport the setup to the test site easily.

4.5 Discussion

Now, the results are discussed based on requirements, and also a comparison is made with the previous prototype. The centering mechanism of the new prototype can expand all three dynamic legs to have full contact with the pipe wall and firmly hold the robot without slipping. The problem with the centering mechanism is that it can not fully expand by itself. The top

dynamic leg is not in contact with the pipe wall. A small lift to the center lead shaft is required so that the centering mechanism is completely able to hold the robot stable inside the pipe. The overall structure of the centering mechanism is sturdy. Thus, the 'must have' design objective (a) is achieved.

Placing the impact-echo test setup at a specific distance from the pipe wall is essential for this project. Adding a distance sensor and getting feedback to control the DC motor made this task achievable. This task was done manually in the previous prototype, introducing human error and reducing repeatability. But now the impact-echo test setup can consistently make an impact from a specified distance with the feedback control implemented in the new prototype. There is still uncertainty of 5 mm offset appearing in the distance readings. Also, sometimes the Arduino COM port stops working when the VL6180X sensor is in operation. The reason for this behaviour is unknown. Thus, the 'must have' design objective (b) is achieved.

Controlling the rotation of the base plate with feedback from the angle sensor makes it possible to make an impact at any desired angle inside the pipe. In the previous prototype, this task was done manually by looking at the robot performing an inspection in the pipe. But in a real scenario, the operator will not see the robot. An angle sensor was already used in the previous prototype, but it was just for the homing of the rotation mechanism. The rotation of the base plate is controlled much effectively using that same sensor. As discussed in the section 4.3, there is an error in the output. To minimize this error, the mechanical play in the lifting mechanism, where there was tilting of the top plate, needs to be removed. Another fix that can be applied is changing the angle sensor's location. The offset will be reduced if it can be mounted on the XZ plane (in line with the impactor arm). Even though the desired angle is not achieved after initial rotation, it is adjusted by the feedback control, and thus the 'must have' design objective (c) is achieved.

The Semi-automatic control routine has improved the repeatability and lead time of the tasks compared to the manual control routine in the previous prototype. The inspection procedure can further be automated by developing a fully automated control routine. Only the pipe diameter needs to be selected initially, and then the complete inspection procedure can be carried out automatically. The new prototype completes the inspection of a section of the pipe in 2 minutes compared to the previous prototype that took 2 minutes and 38 seconds. Even though the current test routine is semi-automatic, the 'must have' design objective (d) is achieved.

The centering mechanism of the new prototype can still not completely center itself inside the pipe. A manual push is required to lift the centering mechanism for the stepper motor's last couple of step counts. So, the 'should have' design objective (a) is not achieved ultimately. A possible solution is to replace the current stepper motor with a motor having higher peak torque. From a structural point of view, the movement of the lead screw nut mount can be guided by metal rods attached to the static leg. It provides more structural strength to the centering mechanism. A mechanism to adapt to pipe diameter can be implemented by using feedback from a pressure sensor attached to the lead screw nut mount (Zhang and Yan (2007)). Another solution is to add a second stepper motor to the other end of the robot. Both motors run the same number of steps but in the opposite direction.

The tilting of the top plate is reduced when rotated compared to the previous prototype. It is achieved by minimizing the mechanical play in the lifting mechanism. Tilting is still not eliminated. There is still some mechanical play because of the loose connection between the links and the base plate. Tightening these loose joints generates more friction between the pin and the slot in the base plate and thus completely restricts the motion of the scissor lift. So, a trade-off needed to be made between completely removing the mechanical play to eliminate tilting or allowing the scissor lift to be lifted. So, the 'should have' design objective (b) is also partially achieved.

Re-arranging the electronic components and replacing the huge stepper motor drivers with a compact motor driver shield made it possible to place all the electronics on the robot itself. It solves two problems. First, mounting all the electronics on-board made the robot portable and easy to transport. As all the electronics are on board, the wires are shortened, which reduces the power loss along the cable. Even though most electronic components are mounted under the base plate, there is enough space for the rotation without colliding with the pipe wall or without any wires tangling. Therefore, the 'should have' design objective (c) is achieved.

The Omni wheels added in the new prototype allow free movement of dynamic legs to expand inside the pipe. These Omni wheels are fabricated in the Lab. It works fine in the PVC pipe and not well in the concrete pipe. Their build quality is not as good as those available in the market. The decision to fabricate the Omni wheels in the Lab was taken because the required wheel size was unavailable in the market. However, the 'should have' design objective (d) is achieved.

Sagging at the middle part of the robot is directly related to the overall length of the robot. The overall length of the robot is reduced by 200 mm in the new prototype, which reduced the sagging by a significant amount. The remaining sagging is compensated by the distance sensor used for the lifting mechanism. Thus, the 'could have' design objective (a) is achieved.

As this prototype only generated the stress wave in the sewer pipe wall, it is not a standalone device to perform the complete impact-echo test. So, to capture the echo reflected from the sewer pipe, a transducer needs to be placed near the impact point. After the signal acquisition, data analysis is done on a computer.

The experiment's conclusion in the concrete pipe is the same as that of the PVC pipe except for the centering mechanism. Due to the roughness of the concrete structure, the Omni wheels cannot freely expand. It is because of the design of the Omni wheel. The rollers of the Omni wheels are spaced far apart from each other. So, the rim of the Omni wheel touches the pipe wall. It is not possible to manually rotate every Omni wheel so that the rollers are in contact with the pipe wall. So, a new Omni wheel needs to be placed with small rollers placed close to each other. Apart from this, the friction generated by the Omni wheels on the concrete surface was considered in the design calculations because it was difficult to determine the coefficient of friction for this application.

A microphone was temporarily placed near the impact point in the concrete pipe test, and the echo was captured. A decibel meter was kept near the microphone, and the loudness of the sound was >85 dB which is enough to analyze the cracks in the pipe or voids around it. Other loud sound source close to the impact is heavy rainfall that is 70 dB. So, the sound of the impact can be distinguished from other sounds.

5 Conclusions and Recommendations

This chapter elaborates the conclusion of the design and performance of the new prototype as well as the further recommendations.

5.1 Conclusions

The new prototype almost satisfies every major design objective defined in Chapter 1. The conclusion based on every design objective are shown below:

- The centering mechanism design is improved so that the dynamic legs adapt to variable pipe sizes and align the central axis of the robot with the pipe center. But this mechanism only works partially. A manual push is required to center the robot inside the pipe entirely.
- The impact-echo setup platform can be precisely placed at a distance from the pipe wall using a distance sensor. A position feedback controller is implemented for the lifting mechanism. The impact can be made consistently from a desired distance on the pipe wall.
- Precise rotation of the impact-echo setup inside the pipe is made using the angle sensor. The impact can be made at multiple angles inside the pipe to be inspected thoroughly.
- A semi-automatic control routine is developed to automate the inspection procedure. This control routine reduces human error, and the precise movement of mechanisms ensures the reliability of the impact-echo test.
- The tilting of the lifting mechanism is reduced when rotated compared to the previous prototype, but it is not eliminated. Any mechanical play in the mechanism is undesirable to control the mechanism precisely. The effect of tilting is compensated feedback control of the rotating mechanism.
- The electronic components are minimized, and cable optimization is done. With all electronics on board, the setup is more portable. The portability of the robot is essential when transporting it to different inspection locations.
- The new Omni wheels reduce the friction between the wheels and the pipe wall. Omni wheels allow smooth lateral movement of the dynamic legs inside the pipe.

5.2 Recommendations

Based on the conclusion made above, things which can be still improved in this prototype are:

- Identify the problem in the centering mechanism and improve it further. Provide a pressure sensor behind the lead screw nut and adjust the force required to push the legs so that the robot centers itself inside the pipe. Consider the friction between wheel and the concrete pipe wall and re-calculate the required torque.
- Change the Omni wheel design or replace it with another type of wheel which further reduces the friction.
- Make the overall robot structure more robust by having aluminum extrudes as the primary support structure for the robot.
- Bigger center lead shaft may provide structural strength to the robot and reduce the sagging problem.

- Eliminate the mechanical play from the robot, especially from the lifting mechanism, to have precise movement control. Also, remove the backlash from the lead screw nut pair.
- Check the possibility of re-designing the impactor arm setup by reducing its length so that the overall length of the robot decreases and the robot is more compact.
- Develop a fully automatic control routine.
- Place a camera module on the inspection robot to get rid of a separate robot for it.
- Mobilize the robot by powering up the wheels. This will help move the inspection robot inside the pipe independently.

A Impact-echo method

The impact-echo method uses non-destructive testing of concrete and masonry structures. Impact-generated stress (sound) waves propagate through concrete and are reflected back by internal flaws and external surfaces. This method is mainly used to determine the flaws such as cracks in the pipe and voids around the pipe.

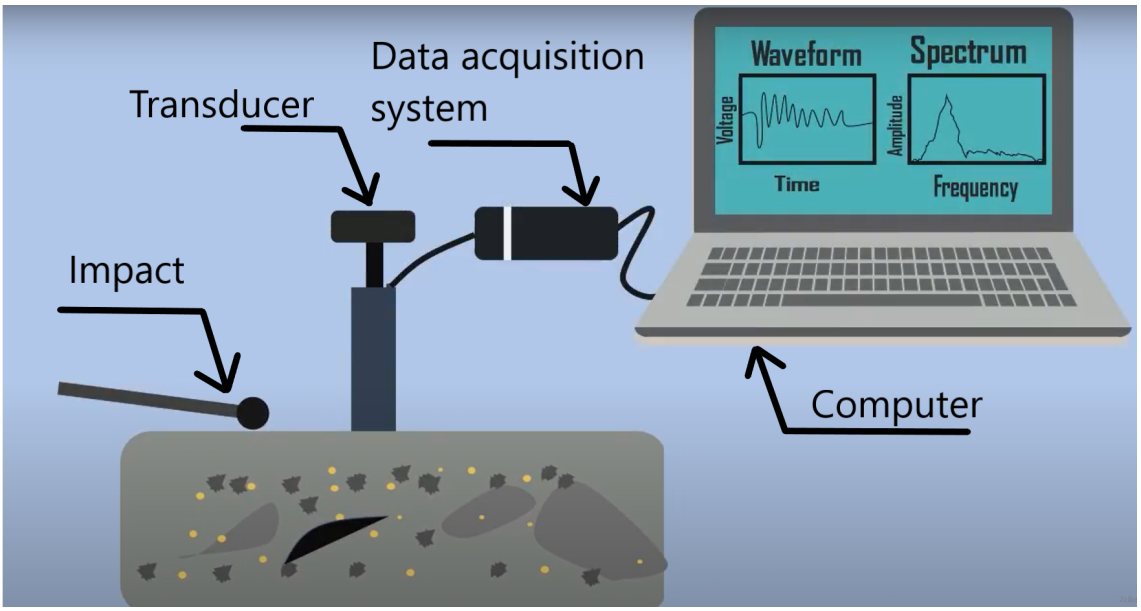

Figure A.1: Simplified diagram of the Impact-Echo method (AnimeEdu (2018))

The Figure A.1 shows an overview of the steps involved in the impact-echo method. Stress (sound) waves are generated at the surface of the concrete through mechanically induced impact. For the source, a steel ball or an impact hammer is typically used. Upon impact, it generates three types of stress waves: Pressure (P), Shear (S) and Rayleigh (R) waves (Pleijsier (2019)). These waves propagates away from the impact point into the structure and are reflected back by flaws and/or external surfaces. P wave consists most useful information on the quality of the medium and the impedance contrast at the interface (Kang et al. (2017)). Surface displacements caused by reflections of these waves are recorded by a transducer located near the impact point. In general, the distance from the impact point to the receiver should be from 20% to 50% of the depth of the shallowest reflecting interface to be measured (Carino (2015)). Stroet (2020) have developed a setup in RaM to generate stress waves in the concrete structure. This same setup is used for this prototype. To develop a mechanism for making impacts, parameter like the weight and size of the steel ball, length of the impactor arm, the spring constant of the torsional spring, and the velocity with which the impact is to be made are determined by Stroet (2020). To have consistent impacts, the distance from the point of release of the steel ball to the impact point needs to be strictly maintained. Stroet (2020) concludes from his experiments that in order to detect deformities in the pipe structure or voids around it, this distance needs to be 40 mm. This distance is used to precisely place the impact-echo test platform close to the pipe wall.

Figure A.2 shows the impact-echo test setup used for this thesis. A steel ball is used to make an impact. The steel ball is attached to a lever arm (impactor arm). A torsion spring is attached at the fulcrum point of the impactor arm. The motion of the impactor arm is controlled by the servo motor. The solenoid is magnetised and the steel ball is put close to it using the servo motor. Then, the servo motor arm is placed to a position where it does not obstruct the impactor

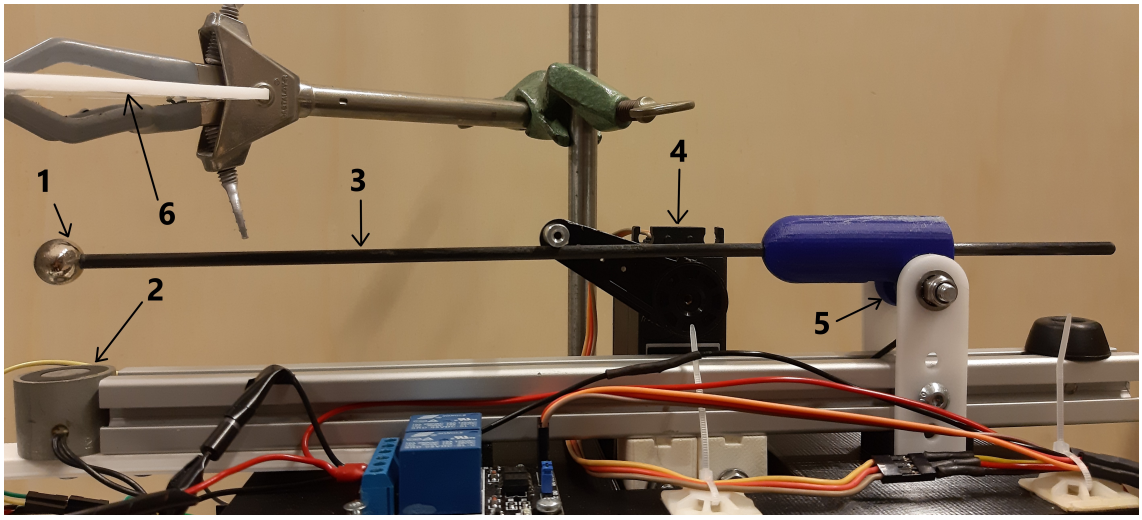

Figure A.2: Impact-echo test setup
1. Steel ball 2. Solenoid 3. Impactor arm 4. Servo motor 5. Torsion spring 6. Impact surface

arm. Finally, as soon as the solenoid is demagnetised the impactor arm is released because of the torsion spring and the steel ball hits the surface making an impact. So, this is the working procedure of making an impact on the sewer pipe wall.

B Torque calculations for lifting mechanism

This section shows the calculations for the torque required to raise and lower the load in lifting mechanism. Torque required to raise the load is derived in Stanley (2012) and is given as

$$Torque\ \ raise \qquad T_r = \frac{W d_m}{2} \tan(\lambda + \phi) \tag{B.1}$$

In above equation, W is the total weight on the top plate, d_m is the nominal diameter of the lead screw, λ is the lead angle and ϕ is the angle of friction. Total weight on the top plate is 0.72 kg.

$$Nominal\ \ diameter \qquad d_m = d - \frac{p}{2}$$

where, d is the diameter of the lead screw and p is the pitch

$$\text{d = 8 mm; p = 8 mm}$$

$$d_m = 8 - 8/2 = 4mm$$

$$lead\ \ angle \qquad \lambda = \tan^{-1}\left(\frac{lead(p)}{\pi d_m}\right) = \tan^{-1}\left(\frac{8}{\pi \times 4}\right) = 25.29°$$

Angle of friction $\phi = \tan^{-1}(\mu)$, where μ is the co-efficient of friction between steel lead screw and brass nut and it taken as 0.15. Therefore, $\phi = \tan^{-1}(0.15) = 8.53°$.

Hence, from equation B.1, $T_r = 0.96N \cdot m$

Similarly, torque required to lower the load is given by,

$$Torque\ lower \qquad T_l = \frac{W d_m}{2} \tan(\phi - \lambda) \tag{B.2}$$

Putting values in above equation, $T_l = 0.53N \cdot m$

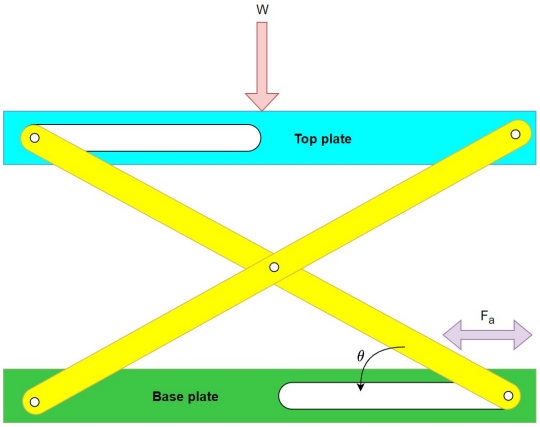

(a) Schematic Overview of the lifting mechanism

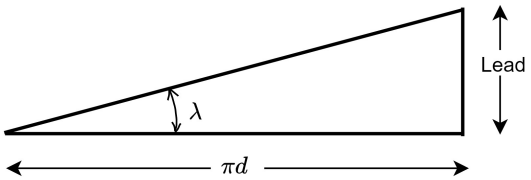

(b) Schematic of lead screw thread

Figure B.1: Scissor lift

C Distance sensor comparison

This section shows the comparison of different distance sensors tested before finalizing the Time-of-flight distance sensor for this project. These comparison includes ultrasonic sensor (HC-SR04), IR sensor (SHARP GP2Y0A41SK0F) and Time-of-flight (ToF) distance sensor (VL6180X). The test setup for the distance measurement is shown in Figure C.1.

Figure C.1: Distance sensor test setup

A series of distance readings are taken from 10 mm to 200 mm at regular interval of 10 mm. The comparison of all sensors is shown in Figure C.2. The reflecting surface is a plain white surface with goof reflectance. From the figure, it can be seen that ultrasonic sensor (orange) starts giving close to accurate results from 30 mm and it always measures a few millimeters less than the actual distance. But ultrasonic sensor does not give accurate readings with a uneven surface like a concrete surface. So, it cannot be used for sewer pipe inspection. Then, the IR sensor (grey) also does not perform well up to 30 mm. But it gives pretty accurate results in the range from 40 mm to 100 mm and then the readings are not quite reliable. The overall performance of the IR sensor is better than ultrasonic sensor but is still not consistent enough. Finally, the ToF distance sensor (yellow) has a constant offset of a few millimeters up to 100 mm and then from 110 mm the readings are very accurate. VL6180X sensor has a good repeatability which is required for impact-echo inspection method. As the sensor module is very small, the IR ray is very narrow which makes sure that line of sight of the sensor is almost straight. As the IR ray is very narrow and the line of sight is almost straight, it helps to measure the exact distance on the curvature of the pipe.

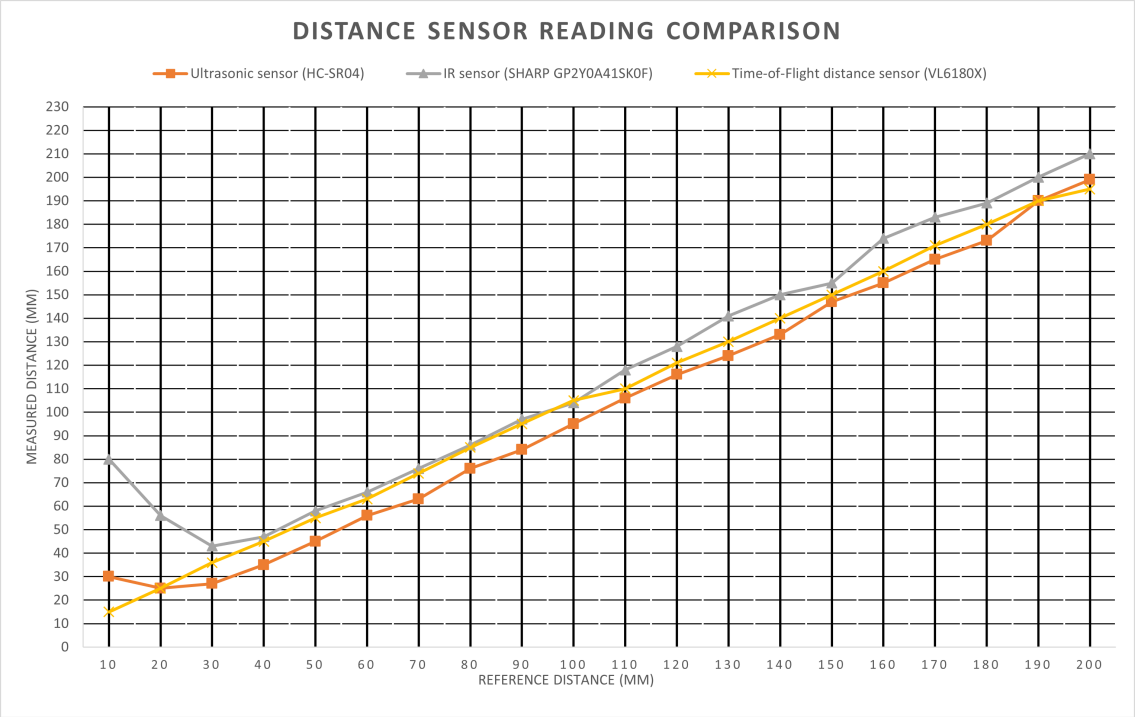

Figure C.2: Distance sensor measurement comparison

D Buttons Logitech controller

Table D.1 and table D.2 gives an overview of the buttons on Logitech F310 game controller used in manual routine and semi-automatic routine respectively.

Table D.1: Serial buttons Logitech controller Manual routine

Controller button	Name	Manual routine
A	buttonA	Servo IN
B	buttonB	Release hammer
X	buttonX	Servo at start
Y	buttonY	Servo at park
Start	Startbutton	Homing
Back	Backbutton	-
Arrow up ↑	DPAD_UP	Lift up
Arrow down ↑	DPAD_DOWN	Lift down
Arrow left ←	DPAD_LEFT	-
Arrow right →	DPAD_RIGHT	-
Mode	Mode	-
LT	RBbutton	Centering
RT	LBbutton	De-centering
LB	LTbutton	Rotating CW
RB	RTbutton	Rotating CCW

Table D.2: Serial buttons Logitech controller Semi-automatic routine

State Description	Controller button	Semi-automatic routine
State 0: pipe selection	A	pipe diameter : 350 mm
	B	pipe diameter : 400 mm
	X	pipe diameter : 450 mm
	Y	pipe diameter : 500 mm
State 1: Homing	Start	perform homing
State 2: Centering	LB	perform centering based on selected pipe size
State 3: Lifting	Arrow up ↑	Automatic lifting up to specified distance
State 4: Impact	LT	Perform automatic impact test procedure
State 5: De-lifting	Arrow down ↓	perform lift homing
State 6: Rotation	Arrow left ←	perform impact test at 90 deg clockwise (state 3 to 5)
	Arrow right →	perform impact test at 90 deg anti-clockwise (state 3 to 5)
	Arrow down ↓	perform impact test at bottom (state 3 to 5)
State 7: De-centering	RB	perform de-centering

E Stepper motor step count calculations

E.1 Centering mechanism step count

This section shows the calculations of the step count for the stepper motor used for centering mechanism. The micro step resolution for this motor is set to 1/8 mode, which means 1600 steps per revolution of the lead screw. The steps are calculated for pipe diameter of 400 mm, 450 mm, and 500 mm. As the homing position of the centering mechanism itself fits the robot inside a 350 mm diameter pipe, there is no need to calculate steps required for stepper motor. The pitch (lead) of the lead screw is 8 mm. Here, it means for 1600 steps of stepper motor, the linear distance travelled by the nut is 8 mm. The figure E.1 shows the schematics of centering mechanism.

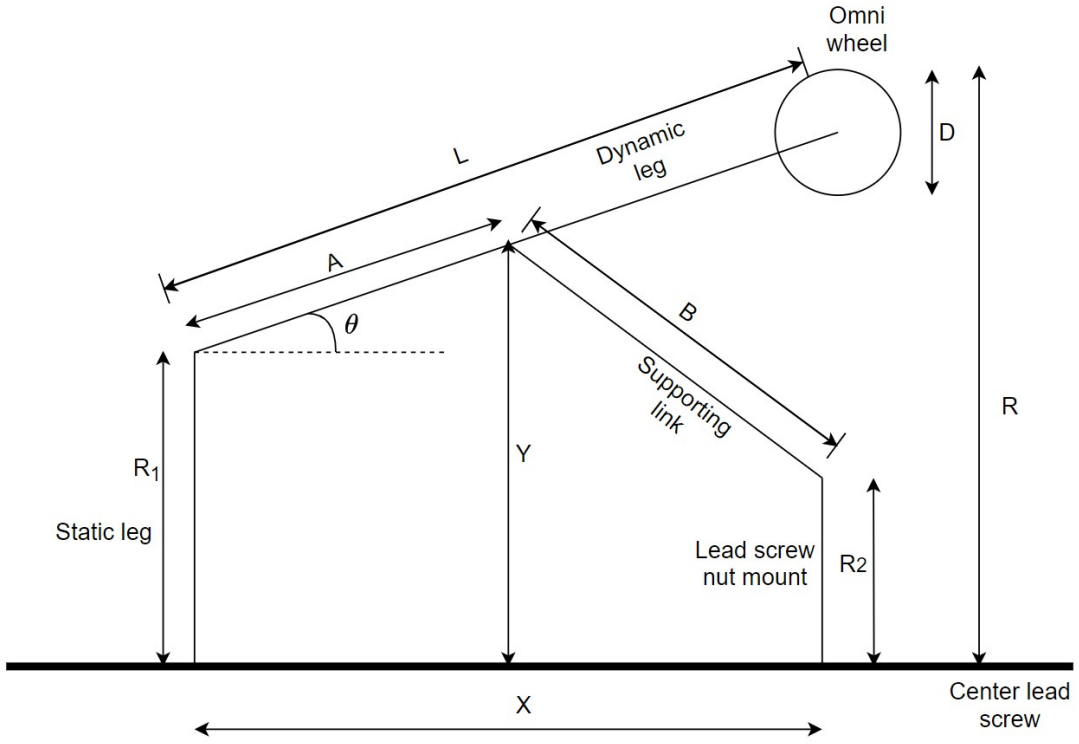

Figure E.1: Schematics of Centering Mechanism

The values for terms in the figure above are as follows: Length of dynamic leg (L) = 144 mm, half-way point (A) = 72 mm, length of supporting link (B) = 114 mm, distance from center lead shaft to top of nut mount (R_2) = 69 mm, distance from center lead shaft to top of static leg (R_1) = 107 mm, θ is the angle of dynamic leg with respect to ground, diameter of the Omni wheel (D) = 48 mm, R is the distance from center lead shaft to the Omni wheel, Y is the distance from lead shaft to point connecting supporting link to the dynamic leg, and X is the distance between static leg and nut mount.

Case 1: pipe diameter 350 mm

$R = 175mm$, $R - R_1 = 68mm$, $R - R_2 = 106mm$

$$\sin\theta = \frac{R - D/2 - R_1}{L} = 0.3055 \quad \therefore \theta = 17.79^\circ$$

$$\cos\theta = 0.9522$$

$$Y = R_1 + A(\sin\theta) = 107 + 72 \times 0.3055 = 129mm$$

$$X = A\cos\theta + \sqrt{B^2 - (Y - R_2)^2} = 165.5mm$$

Case 2: pipe diameter 400 mm

$R = 200mm$, $R - R_1 = 93mm$, $R - R_2 = 131mm$

$$\sin\theta = \frac{R - D/2 - R_1}{L} = 0.4791 \quad \therefore \theta = 28.63^\circ$$
$$\cos\theta = 0.8777$$

$$Y = R_1 + A(\sin\theta) = 107 + 72 \times 0.4791 = 141.5mm$$

$$X = A\cos\theta + \sqrt{B^2 - (Y - R_2)^2} = 151.17mm$$

The distance nut mount have to travel is 165.5 - 151.17 = 14.33 mm. Therefore, steps needed by stepper motor to travel this distance is 2866.

Case 3: pipe diameter 450 mm

$R = 225mm$, $R - R_1 = 118mm$, $R - R_2 = 156mm$

$$\sin\theta = \frac{R - D/2 - R_1}{L} = 0.6527 \quad \therefore \theta = 40.75^\circ$$
$$\cos\theta = 0.7575$$

$$Y = R_1 + A(\sin\theta) = 107 + 72 \times 0.6527 = 154mm$$

$$X = A\cos\theta + \sqrt{B^2 - (Y - R_2)^2} = 130.5mm$$

The distance nut mount have to travel is 165.5 - 130.5 = 35 mm. Therefore, steps needed by stepper motor to travel this distance is 7000.

Case 4: pipe diameter 500 mm

$R = 250mm$, $R - R_1 = 143mm$, $R - R_2 = 181mm$

$$\sin\theta = \frac{R - D/2 - R_1}{L} = 0.8263 \therefore \theta = 55.73^\circ$$
$$\cos\theta = 0.5631$$

$$Y = R_1 + A(\sin\theta) = 107 + 72 \times 0.8263 = 166.5mm$$

$$X = A\cos\theta + \sqrt{B^2 - (Y - R_2)^2} = 99.61mm$$

The distance nut mount have to travel is 165.5 - 99.61 = 65.9 mm. Therefore, steps needed by stepper motor to travel this distance is 13,178.

E.2 Rotating mechanism step count

The rotation mechanism uses the angle sensor MPU-6050 for its movement. The stepper motor for the rotating mechanism is also set to 1/8 mode. The calculations for getting roll angle from sensor data is taken from the master thesis of Zwiep (2021). Here, the driver gear have 20 teeth and driven gear have 60 teeth, so the ratio n = 3. The step count needed for the rotation mechanism are for angles 90° and 180°. The number of revolutions and number of steps needed to complete the rotation of the mechanism is calculated by equations

$$number\ of\ revolutions = \frac{\theta n}{360} \tag{E.1}$$

$$number\ of\ steps = number\ of\ revolutions\ \frac{steps}{rev} \tag{E.2}$$

For θ = 90°, steps needed are 1200 and for θ = 180°, steps needed are 2400. These steps count are calculated assuming the position of the MPU-6050 close to the rotation axis.

F Electrical circuit diagram

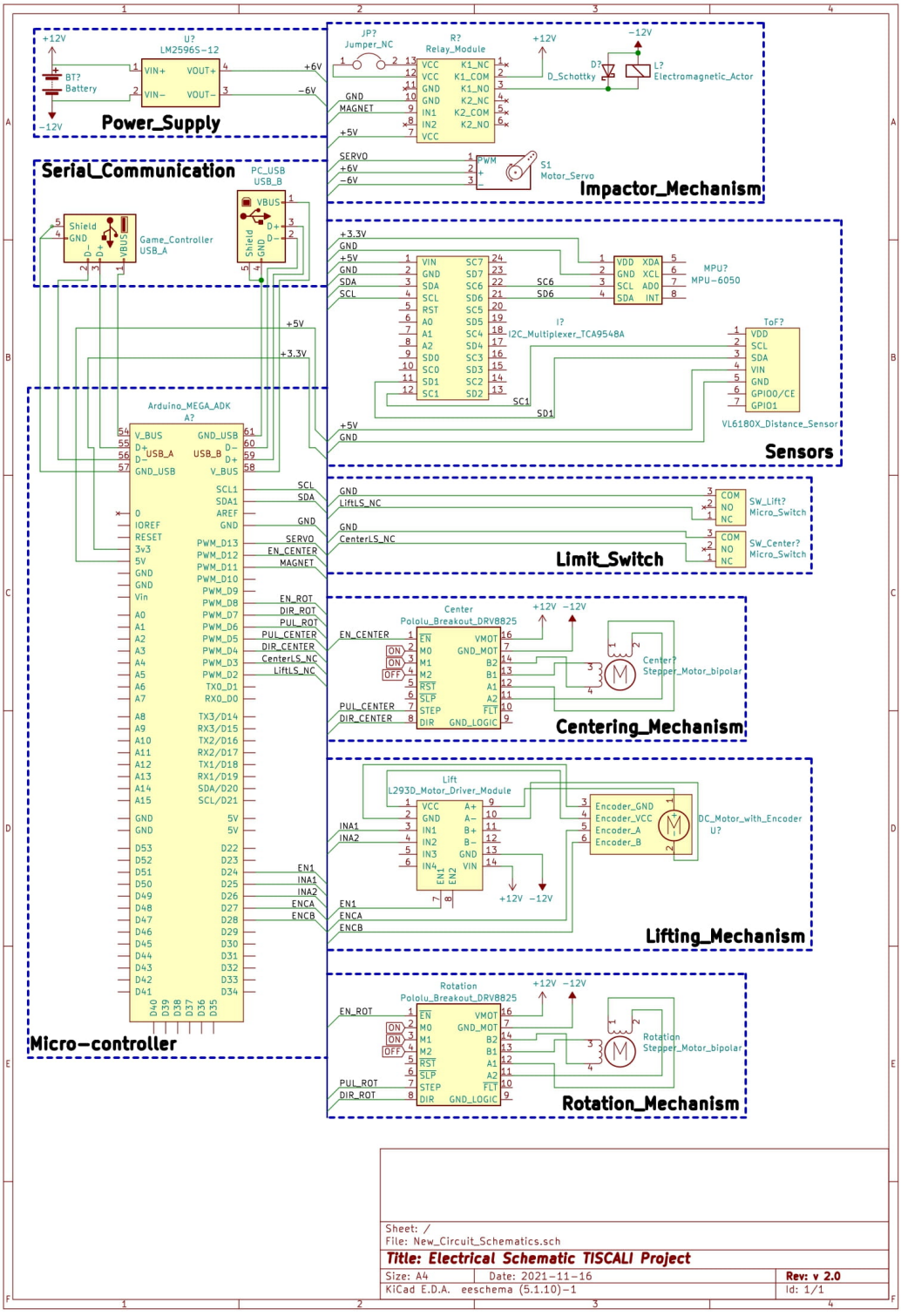

Figure F.1: Electrical circuit of the new prototype

Bibliography

AnimeEdu (2018), Impact-Echo Test for concrete.
https://www.youtube.com/watch?v=Dif-hj1eCM4

Bin Ibrahim, A. N., P. Bin Ismail et al. (2002), *Guidebook on non-destructive testing of concrete structures*, volume 17, INTERNATIONAL ATOMIC ENERGY AGENCY (IAEA), Wagramer Strasse 5, A-1400 Vienna, Autria.
https://www-pub.iaea.org/mtcd/publications/pdf/tcs-17_web.pdf

Carino, N. J. (2015), Impact Echo : The Fundamentals Principles of Impact-Echo Method, *International Symposium Non-Destructive Testing in Civil Engineering (NDT-CE)*.

Davies, J. P., B. A. Clarke, J. T. Whiter and R. J. Cunningham (2001), Factors Influencing the structural deterioration and collapse of rigid sewer pipes, *Elsevier*, pp. 73–89.

Dertein, E. (2015), TISCALI : Technology Innovation for Sewer Condition Assessment – Long-distance Information-system.
https://www.ram.eemcs.utwente.nl/research/projects/tiscali

Feng, G., Z. Li, Z. He, Y. Feng, T. Xue and K. Liu (2016), Effect of high pressure water jet cleaning device on the motion stability of an in-pipe cleaning robot, *IEEE International Conference on Robotics and Biomimetics*, pp. 1040–1045, doi:10.1109/ROBIO.2016.7866462.

Fisher, J. C. (2010), Using an Accelerometer for Inclination Sensing.
https://www.analog.com/media/en/technical-documentation/app-notes/an-1057.pdf

Ismael, O. Y., M. Almaged and A. Mahmood (2019), Quantitative Design Analysis of an Electric Scissor Lift, in *American Scientific Research Journal for Engineering, Technology, and Sciences (ASRJETS)*, volume 59, pp. 128–141, ISBN 2313-4402.

Kakogawa, A. and S. Ma (2010), Mobility of an in-pipe robot with screw drive mechanism inside curved pipes, in *IEEE International Conference on Robotics and Biomimetics, ROBIO 2010*, pp. 1530–1535, ISBN 9781424493173, doi:10.1109/ROBIO.2010.5723557.

Kang, J. M., S. Song, D. Park and C. Choi (2017), Detection of cavities around concrete sewage pipelines using impact-echo method, *Tunnelling and Underground Space Technology*, **vol. 65**, pp. 1–11, ISSN 0886-7798, doi:http://dx.doi.org/10.1016/j.tust.2017.02.002.

Min, J., Y. D. Setiawan, P. S. Pratama, S. B. Kim and H. K. Kim (2014), Development and controller design of wheeled-type pipe inspection robot, in *Proceedings of the 2014 International Conference on Advances in Computing, Communications and Informatics, ICACCI 2014*, pp. 789–795, ISBN 9781479930791, doi:10.1109/ICACCI.2014.6968543.

Noshahri, H., L. o. S. Léon and G. D. Andre (2021), Linking sewer condition assessment methods to asset managers' data-needs, *Automation in Construction, Elsevier*, submitted.

Petrescu, V., A. Petrov, I. El-Hajj, V. R. Son and G. Gransden (2017), Omni-wheel friction coefficient measuring methodology for various angles, *ASML B.V.*, **vol. 10**, pp. 1–10.
https://vladpetrescu.files.wordpress.com/2017/10/asml_article.pdf

Pleijsier, A. (2019), *Acoustic Condition Assessment of Concrete Sewer Pipes using a Particle Velocity Sensor*, Ph.D. thesis, University of Twente, Enschede, The Netherlands.

Stanley, M. (2012), *SCISSOR LIFT DESIGN FOR USE IN THE AUTOMOTIVE INDUSTRY*, Master's thesis, Niger Delta University, Wilberforce Island, Amassoma, Beyelsa state.

Stroet, J. (2020), *Impactor Design for In-pipe Impact-echo Inspection Method: A Morphological Analysis*, Master's thesis, University of Twente, Enschede, The Netherlands, robotics and Mechatronics group, EEMCS.

Wahed, M. A. A. and M. R. Arshad (2017), Wall-press type pipe inspection robot, in *Proceedings - 2017 IEEE 2nd International Conference on Automatic Control and Intelligent Systems, I2CACIS 2017*, pp. 185–190, doi:10.1109/I2CACIS.2017.8239055.

Zhang, Y. and G. Yan (2007), In-pipe inspection robot with active pipe-diameter adaptability and automatic tractive force adjusting, *Mechanism and Machine Theory*, **vol. 42**, pp. 1618–1631, ISSN 0094114X, doi:10.1016/j.mechmachtheory.2006.12.004.

Zwiep, L. (2021), *Mechatronic solution for stress-wave generation using impact echo*, Master's thesis, University of Twente, Enschede, The Netherlands, robotics and Mechatronics group, EEMCS.